Strengthening Resilience of Electric Power Distribution Systems against Natural Disasters: A Perspective from Machine Learning and Optimization

by

Zheming Liang

A dissertation submitted in partial fulfillment
of the requirements for the degree of
Doctor of Philosophy
(Electrical and Computer Engineering)
in the University of Michigan-Dearborn
2020

Doctoral Committee:

Associate Professor Wencong Su, Chair
Assistant Professor Junho Hong
Assistant Professor Ruiwei Jiang, University of Michigan
Assistant Professor Mengqi Wang

2020

This thesis is proudly dedicated to my dear father and mother, *Liang Tian Jie* and *Sun Yan*, who have supported me from the beginning of my life.

ACKNOWLEDGEMENTS

I would like to express my greatest gratitude to my advisor Dr. *Wencong Su*. I first met with him when I was pursuing my master degree in the University of Michigan-Dearborn in Fall 2013, when we discussed our future careers in his office. Then I started to pursue my Ph.D degree in Oklahoma State University till the year of 2016. Due to lack of funding, I have to change my advisor and apply again to continue my Ph.D study. Dr. *Wencong Su* is my best option and fortunately he offered me a GSI position to ensure that I have sufficient funding to carry on my Ph.D study.

In addition, I would like to thank my Ph.D committee member Dr. *Ruiwei Jiang* (IOE Department, Ann Arbor Campus), Dr. *Mengqi Wang* (ECE Department), and Dr. *Junho Hong* (ECE Department) for their valuable comments and advices regarding the preliminary exam.

Moreover, I would like to thank the committee members of my qualify exam, Dr. *Kevin Bai* (Assistant Professor in UTK) and Dr. *Teahyung Kim* (ECE Department) for their helpful advice and constructive comments on my research work.

Furthermore, I would like to thank Dr. *Di Shi*, Dr. *Desong Bian* and Dr. *Xiaohu Zhang* for offering the summer research associate internship in GEIRINA in the year of 2018 and 2019. Without their help, I could not achieve where I am now in the area of energy management for commercial systems.

Lastly, I would like to thank Dr. *Paul Richardson*, *Mariann Brevoort* and *Amanda Donovan* for their help since when I first entered the department in the year of 2011.

TABLE OF CONTENTS

LIST OF FIGURES

LIST OF TABLES

ABSTRACT

The resilience issues in the power system have attracted increasing attention worldwide, especially for the distribution systems that suffer from extreme weather events, such as hurricanes and wildfire. In this dissertation, several novel algorithms, such as safe reinforcement learning algorithm and risk-constrained adaptive robust optimization approach are proposed to provide resilient proactive scheduling strategies, emergency response strategy and restoration strategy for central controllers in the distribution system. Microgrids are proposed to serve as single entities from the perspective of the distribution system operator to enhance the resilience of the distribution system, reduce the distribution system operator's control burden and improve the power quality of the distribution system. Uncertainties related with the extreme weather events such as power generation of distributed generators, intermittent load demand, point-of-common-coupling/tie-line conditions, and trend/trace of the extreme weather event are tackled through a combination of optimization approaches, artificial intelligence algorithms and risk management methods. Extensive simulation results based on real-world data sets show that the proposed novel algorithms based proactive scheduling strategies, emergence response strategy and restoration strategy can ensure the resilience of the distribution system in a real-world environment.

CHAPTER 1

Introduction

In this chapter, we first introduce the basic concept of power system and the detailed components within a power system. Then, the importance of the distribution system is highlighted to ensure the resilience and reliability of the power consumption with the help of distributed energy resources (DERs) and microgrids. In addition, various optimization algorithms and machine learning methods are introduced to handle the uncertainties associate with the extreme weather event. Moreover, we compared prior works with our works in ensuring the resilience of the distribution system through various optimal control strategies in different stages.

In the Chapter 2, the proposed resilient proactive scheduling strategy for major components within a commercial building (CB) in a distribution system are demonstrated, where a safe reinforcement learning (SRL) based algorithm is proposed to handle the uncertainties associated with the extreme weather events. The combination of risk management method with deep reinforcement learning (DRL) algorithm is developed to tackle the uncertainties and risks associated with the extreme weather events. Uncertainties related to the extreme weather events includes power generation of distributed generators (DGs), intermittent load demand, point-of-common-coupling (PCC)/tie-line conditions, and trend/trace of the extreme weather event, etc.. Several novel models of the comprehensive comfort levels and correlated demand response (CDR) with in a CB are developed to capture the unique features of the major components within the CB. Extensive simulation results based on real-world data sets validate the effectiveness of the proposed resilient proactive scheduling strategy in ensuring the resilience of a CB in the distribution system.

In the Chapter 3, the proposed resilient proactive scheduling strategy for major components within independent/networked microgrids in a distribution system are demonstrated, where a two-stage (pre-event and real-time) risk-constrained adaptive robust optimization (RARO) approach is proposed to handle the uncertainties associate with the extreme weather event. The combination of risk management method with optimization approach is developed to tackle the uncertainties and risks associated with the extreme weather events. Uncertainties related to the extreme weather events includes power generation of distributed generators (DGs), intermittent load demand, point-of-common-coupling (PCC)/tie-line conditions, and trend/trace of the extreme weather event, etc..

Several novel models of the microgrids are developed to capture the unique features of the major components within the microgrids. Extensive simulation results based on real-world data sets validate the effectiveness of the proposed resilient proactive scheduling strategy in ensuring the resilience of the independent/networked microgrids in a distribution system.

In the Chapter 4, a comprehensive framework to provide resilient restoration decisions for the distribution system operator (DSO) under extreme events is proposed. Our objective is to maximize the system resilience by minimizing time slots required for load restoration. Bat algorithm is used to handle nonlinear and discrete characteristics of the proposed framework. Extensive simulation results show that the approach we proposed can ensure the resilience of the distributed system.

In the Chapter 5, the contributions of the dissertation are summarized. In addition, there are still challenges that remain in the emergency response stage, such as the issues of situation awareness, dispatching a rescue team, and relay protection. I will continue my study on the highly correlated uncertainties associate with the extreme events in the future research. I will develop a novel method with the vine copula approach to describe the dependence between various uncertainties and reduce the total dimension of the resilience related problems.

1.1 Power System

The primary propose of the power system is to deliver the generated electricity from the conventional fuel-based power plants to the consumers/end users. As shown in Fig. 1.1, the power

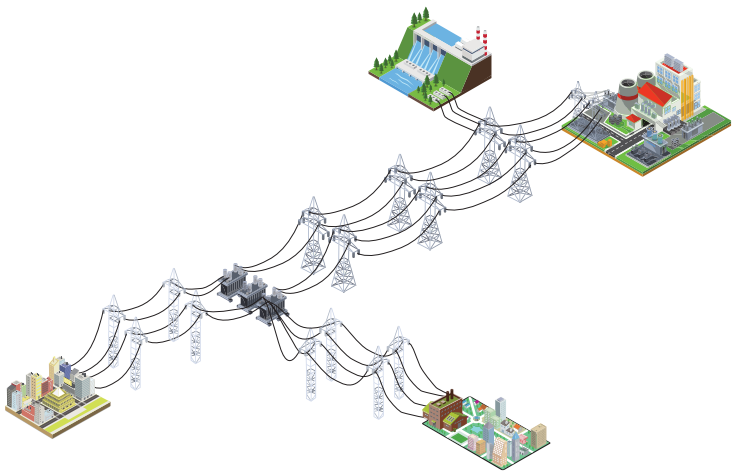

Figure 1.1: A big picture of the power system.

system can be divided into four main sections, namely generation system, transmission system, distribution system and consumption. In the conventional power system, a large portion of the energy is produced in the generation section through power plants. Then the generated energy is

transmitted through transformers to increase the voltage magnitude for reducing the transmission loss. After that, the ultra high voltage energy is transmitted through transmission lines to the distribution system, where the voltage level will be downgraded from 750 kV/500kV to 110kV/35 kV. This is the system closest to the end user side, which has great impact on the power quality and reliability. More importantly, the distribution system has the duty to make energy accessible to all users, which significantly increased the control burden of the conventional distribution system operators. The economy, national security and even the health and safety of the people depend on the reliable delivery of electricity. However, the electric infrastructure in the U.S. is aging and its being pushed to do more than it is designed originally. Modernizing the power system will make it smarter and more resilient by technologies, equipments and optimal control strategies. This modernizing provides more opportunities for the conventional independent system operators (ISOs) and distribution system operators (DSOs) but it also makes the system more complicate and changes its configuring, especially for the distribution system. The details are explained in the following sections:

1.1.1 Generation

The generation of the electricity can be classified into two categories, namely: renewable energy sources (RES) based generation and non-renewable fuel based generation. For RES based generation units, they mainly refer to solar panels and wind turbines to form the wind farm as well as the solar station. For non-renewable fuel based generation units, they mainly refer to coal-based generators, gas-based generators and nuclear power based generators to form the conventional power plants. Specifically, most of the spinning reserves are from the coal-fired/gas-based power plants, which are necessary components to ensure the reliability of the power system, especially when huge amount of renewable energy sources based distributed generators are deployed in the distribution system. The trend is to replace the conventional power plants in the generation side which far away from the consumption side by distributed generators (DGs) near the end users side in the distribution system (gas-based combined heat and power (CHP) to improve the overall efficiency), where the frequency issues are tackled by converters with the DGs.

1.1.2 Transmission System

The role for the transmission system in the whole power system is to transmit the generated power from the generation side to the demand side through transmission lines and transformers. The voltage magnitude of the electricity generated from the power plant needs to be scaled up to reduce the transmission losses when transmitting the power in a long distance. In addition, the voltage magnitude needs to be scaled down when reaching the distribution system.

1.1.3 Distribution System

After receiving the power transmitted from the transmission system, the DSO need to first scale down the ultra-high voltage electricity to around 110kV–35kV through the substations and transformers. Then the DSO can dispatch the power to the end user after the calculation of N-2 contingency issues in case of congestions on the distribution lines. However, as mention above, distributed energy resources (DERs) such as distributed storages (DSs), DGs, smart switches (SSs) and controllable loads (Cls) with different capacities and characteristics are vastly deployed in the distribution system. The conventional DSOs are not designed to manage and control such amount of small-scale DERs. Therefore, we need to find a very effective way to handle such issue, where microgrids are introduced into the power and energy society to control the huge amount of DERs through the local controllers.

1.1.3.1 Microgrids

According to the Department of Energy (DOE) of the U.S., a microgrid is a group of interconnected loads and DERs with in clearly defined electrical boundaries that acts as a single controllable entity with respect to the grid and that connects and disconnects from such grid to enable it to operate in both grid-connected or islanded mode. The microgrid is a framework to facilitate the integration and management of DERs in a decentralized way. Microgrids can significantly reduce the control burden of the DSO by allowing local controllers for DERs to coordinate with microgrid central controllers (MGCCs). Also, microgrids can strengthen grid resilience and help mitigate grid disturbances since they are able to continue operating while the upstream grid is down. In addition, microgrids use DER to sere local loads, reduce energy losses and improving the efficiency of distribution systems. Networked microgrids share the same unique features as the independent microgrids. However, they are interconnected through tie-lines, which bring additional challenges for the MGCCs.

1.2 Resilience and Reliability Issues in the Distribution System

In order to preserve a sufficient power supply for a distribution system while islanded from the main grid, the central controller of the microgrids needs to utilize various major components, such as the energy storage system (ESS) and combined heat and power (CHP), to provide reserves during an extreme weather event [1]. In addition, not only is the resilience related to the power supply important, but the heating and cooling resilience should also be considered. This is because the critical loads in a microgrids, e.g., servers, require a constant indoor temperature that is monitored through heating, ventilation, and air-conditioning (HVAC) systems, which makes H-

VAC systems critical loads as well [2]. Note that during certain time slots (even some time slots during an extreme weather event), the power supply to critical loads must be guaranteed. However, energy reserves may not be able to cover the energy imbalance during the entire extreme weather event [3]. Such a challenge requires the central controller to deploy a correlated demand response with proactive resilient reserves to ensure the resilience of the microgrids.

The simple demand response problem for microgrids' reliability issues with/without comfort levels has been extensively studied [4]. That said, the correlation between distributed energy resources (DERs) when performing demand response under a potential extreme weather event while maintaining comprehensive comfort levels has not been considered [5]. For instance, when performing conventional resilient operation with a simple demand response, an HVAC system in a microgrid may shift the work load from 2:00 pm–3:00 pm to 3:00 pm–4:00 pm. At the same time, electric water heaters (EWHs) and plug-in electric vehicles (PEVs) are operating as pre-event scheduled, while an extreme weather event is about to strike the area from 2:00 pm–3:00 pm. Note that the power resilience can be maintained in this case, but the heating/cooling resilience will be affected by the simple demand response process. In order to maintain both the power resilience and the heating/cooling resilience, a framework utilizing both the correlated demand response (CDR) method and proactive resilient scheduling is proposed for the central controller of a micorgrid.

1.2.1 Extreme Weather Events

Extreme events can be classified into two categories, namely extreme weather events and extreme cyber-physical events. Specifically, hurricanes, earthquakes, snowstorms and wild fires are the major forms of extreme weather events that can cause huge blackouts all over the world. Even though the independent system operators have learned their lesson from the 2003 blackout, only $N-1/N-2$ contingency based security conditions have been included in the conventional operation decision making process. Such security criterion is not suitable for a possible extreme weather event, especially for a distribution system that does not have enough spinning reserve to ensure its own resiliency. Thus, many research institute and organizations in the United States such as Electric Power Research Institute (EPRI), Federal Energy Regulatory Commission (FERC) and North American Electric Reliability Corporation (NERC), have proposed several resilient operation strategies for the system operators against potential extreme weather events.

1.2.2 Four Stages

There are four stages associated with the resilience of a distribution system, namely hardening, proactive scheduling, emergency response and restoration stages. It can also be categorized as prior the extreme event, during the extreme event and after the extreme event. The hardening and

restoration aspects have been extensive studied in prior works. Therefore, we mainly focusing on the proactive scheduling and emergency response stages. As shown in Fig. 1.2, the operating status can be treated as numbers of critical loads operating in the steady state. The extreme event occurs at the time t_2, where the first slope between t_2 and t_3 indicates the development of the extreme weather event. As time goes by, the curve becomes flat, which means that the extreme weather event is about to leave the distribution area, where the damage of the extreme event reaches the highest level at that time.

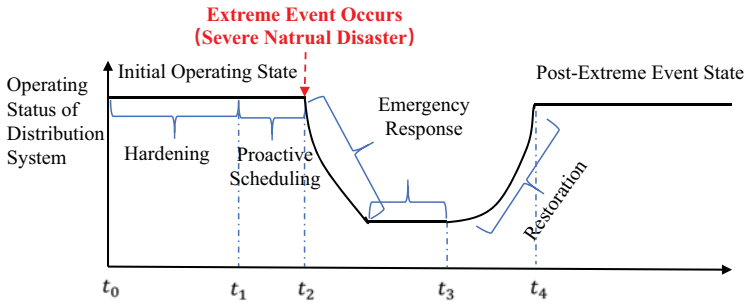

Figure 1.2: The four stages associated with the resilience of a distribution system.

1.3 Optimization Approaches, Artificial Intelligence Algorithms and Risk Management Methods to Handle Uncertainties

With the concept of the extreme weather events, we began to narrow down the possible uncertainties need to be considered in the proactive scheduling stage, emergency response stage and restoration stage, such as when and where the extreme event would occur, which bus or node would be influenced by the extreme weather event, and the intermittent generation and load demand, which are all challenges need to be tackled to ensure the resilience of the distribution system. Some of prior works consider stochastic approach to handle uncertainties which requires a hard-to-obtain probability distribution of each uncertainty which is impossible for the complicate real-world cases and brings a lot of computational burden to the problem [6]. Other prior works consider conventional robust optimization approaches to handle the uncertainties which are too conservative and did not consider the risks associate with the low possibility of high cost. Moreover, for the resilience issues in the distribution system, the uncertainties of the extreme event changes with the time slots. Thus, the adaptiveness of the solution approach is also very important. In addition to the optimization methods, artificial intelligence (AI) based algorithms are also introduced by prior works to consider the uncertainties, such as Markov decision process (MDP), reinforcement learning (RL), and deep reinforcement learning (DRL). However, none of the al-

gorithms mentioned above can fully address all the unique features of the resilience issues in the distribution system.

1.4 Prior Works vs. Our Works

In addition to the aforementioned challenges, extreme weather event related uncertainties, such as grid-connected conditions (including the duration of and when the extreme event will strike a commercial campus), power generation of rooftop solar panels, intermittent load demand in the CB, arrival state-of-charges (SoCs), and arrival/departure time of PEVs, are major obstacles preventing the optimal control decisions from occurring as scheduled. To handle these uncertainties, various optimization algorithms, such as scenario-based stochastic programming [7], robust optimization [8], and distributionally robust optimization [9], have been developed. However, the key feature of an extreme weather event is that the decisions made in the pre-event stage lack adaptiveness to the real-time conditions. To improve the real-time fast response capability of the cental controller in a CB during an extreme weather event, a reinforcement learning (RL) method can be introduced [10], such as the Q-learning method [11]. In addition to Q-learning, which can only handle discrete state and action spaces, a deep Q-network (DQN) has been developed for a continuous state space and a discrete action space [12]. It is suitable for a CB that requires simple actions, such as the on/off actions of an ESS. Furthermore, risks associated with the extreme weather uncertainties need to be tackled during the training process in order to mitigate the influence caused by potential extreme epochs [13]. Thus, a safe reinforcement learning (SRL) algorithm [14] has been developed by combining the DQN method and conditional-value-at-risk (CVaR) method considering all the unique features of the proactive resilient scheduling problem.

Therefore, we proposed several novel proactive scheduling strategies and emergency response strategy based on safe reinforcement learning and risk-constrained adaptive robust optimization approach for the distribution system to ensure its resilience.

CHAPTER 2

Proactive Scheduling Strategies for a Commercial Microgrid in the Distribution System

The detailed studies for the proactive scheduling stage of the major components in the distribution system based on the proposed algorithms and control strategies are demonstrated in these chapters. We first introduce the proposed proactive resilient scheduling strategy for the GEIRINA's commercial building on a commercial campus in San Jose, CA based on safe reinforcement learning algorithm. After that, a risk-constrained adaptive robust optimization is developed to handle the uncertainties for central controllers of networked microgrids in the following chapter.

2.1 Motivations and Contributions

Distribution systems now contribute more to the resilience of the whole power system than ever before, especially in the face of extreme weather events. With the help of microgrids, the potential risks of cascading failures in a distribution system have been minimized. However, such capability highly relies on a strong communication network, which is impossible to maintain when an extreme event (such as a hurricane) strikes. Moreover, the cost to restore the operation of commercial buildings (CBs) to the pre-event phase is much higher than that of restoring residential households [15]. Thus, in order to maintain the resilience of CBs, a technology called proactive scheduling has been developed. Unlike hardening and restoration, which make decisions either years before or months after a potential extreme event, proactive scheduling can provide resilient control decisions several hours before the potential extreme event, which also ensures a satisfaction level regarding the energy demand during the extreme event.

Buildings consume nearly 40% of the annual electricity generation of the United States (U.S.), of which half of total energy consumption is from commercial buildings (CBs) [16]. CBs contribute to a significant portion of the gross domestic product (GDP) in the U.S. Ensuring the reliability of the CBs is a major concern of distribution system operators (DSOs). However, congestion

of transformers and distribution lines in the upstream grid can lead to contingency issues, which pose a significant threat to the reliability of CBs in commercial campuses. To prevent a contingency issue from influencing the reliability of a commercial campus, a controller is needed for the optimal energy management.

Among prior proposed energy management strategies, their objectives can be categorized into three groups: (i) to minimize the operating cost of the system [17]; (ii) to maximize the comfort levels of occupants or minimize the discomfort levels of occupants (mainly related with the indoor temperature) [18]; and (iii) to minimize the load curtailment of the system or maximize the survivability of critical loads [19]. Reference [20] synthetically combines the first two objectives using a stochastic optimization approach. The energy management strategy proposed in [21] considers both operation cost minimization and customer comfort level maximization in a commercial campus. However, the islanding capability of a commercial campus, which is one of the unique features of a microgrid, is not addressed. With the increasing market trend of plug-in electric vehicles (PEVs), an effective energy management system should also handle the uncertainties associated with PEVs [22]. Even though the penetration level of PEV owners among all occupants of CBs is relatively small, the instant charging of PEVs upon arrival can create huge demand ripples, which not only increase the expected operation and maintenance (O&M) costs, but also the possibility of a cascading failure occurring at the point of common coupling (PCC) [23].

The islanding capability of a commercial campus can ensure sufficient energy supply to the critical loads during the uncertain islanding period. Specifically, in the case of microgrid scheduling, the problem of islanding constraints has received considerable attention. A review of existing methods in handling islanding conditions for microgrid central controllers is provided in [24], where the concept of smooth transition between grid-connected mode and islanded mode is discussed. In [25], G. Liu present an optimal scheduling model for microgrid operation taking into account the probabilistic constraints of successful islanding. A chance constraint is proposed to represent the probability of a microgrid maintaining enough spinning reserve to accommodate the demand and renewable energy after islanding from the upstream grid. The authors in [26] utilize the combined heat and power (CHP) units as back-up power and heating sources along with other major components in a microgrid to overcome the energy imbalance caused by the islanding issues. In addition, the possibilities of losing major components are also considered. Voltage imbalance in the microgrid caused by the islanding from the main grid is studied in [27], which utilizes distributed generators and inverters to maintain the voltage magnitude in the islanded mode. Z. Li demonstrate an islanding-aware economic dispatch mechanism for the microgrid central controller to minimize the operating cost in both grid-connected mode and islanded mode [28]. They also present the concept of energy deviation along with its associated costs. None of the aforementioned works, however, has considered all the distinct factors for the optimal energy management

strategy of a commercial campus with islanding capabilities.

In this work, we propose a novel safe reinforcement learning algorithm to provide resilient proactive scheduling decisions for the central controller of a CB. The correlation between different components with demand response capabilities is utilized for the first time to ensure the desired comprehensive comfort levels of the occupants can be maintained by the limited reserves. The trade-off between the demand response amount and the maximum total comfort level of the occupants in the CB is handled by several penetration level indices developed in our prior works. An SRL algorithm is developed through combining a DQN method and a CVaR method to mitigate the influence of extreme epochs in the learning process. Extensive simulation results based on real-world data sets validate that the proposed proactive scheduling strategy based on the developed SRL algorithm is capable of ensuring the resilience of the CB under an extreme weather event.

In summary, we make following contributions in this work:

1. A proactive scheduling strategy is proposed to ensure CB resilience when an extreme weather event occurs.

2. An SRL algorithm is developed through combining a DQN method and a CVaR method to mitigate the influence of extreme epochs, where exploration and exploitation are considered simultaneously.

3. The correlation between different components with demand response capabilities is introduced for the first time to ensure the desired comprehensive comfort levels of the occupants can be maintained by the limited reserves.

4. Extensive simulation results show the effectiveness of the proposed proactive scheduling strategy in minimizing the damage caused by extreme weather events while maximizing the occupants' comfort levels during an extreme weather event.

2.2 System Modeling

In the proposed commercial campus, as shown in Fig. 2.2, there is one CB and one parking lot, which can be scaled to multiple CBs smoothly. In the CB, there is one HVAC system, several EWHs, several ESSs, several rooftop solar panels, several CHPs, and one base load. There are also several PEVs that are owned by the occupants of the CB that need to be charged in the parking lot during office hours. In order to ensure the power balance of the commercial campus throughout the whole operating day, both resilience and reliability related constraints are proposed. There are 96 time slots in each operating day, such that each time slot is 15 minutes. The system modeling is based on the real-world data from the GEIRINA's CB in San Jose, CA as shown in Fig. 2.1.

Figure 2.1: The major components in a commercial campus.

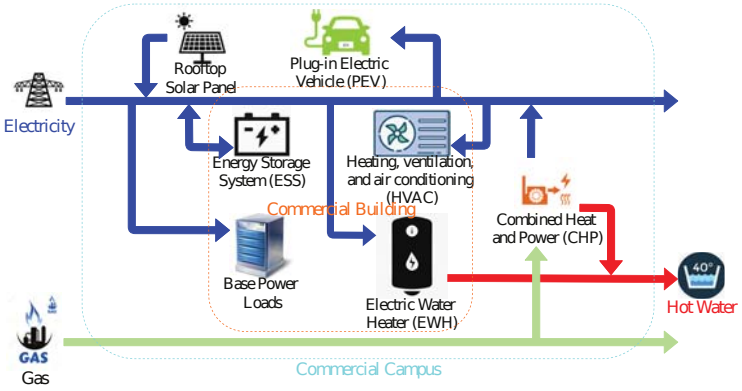

Figure 2.2: The major components in a commercial campus.

2.2.1 Appliance Constraints

This section describes the detailed formulation of each appliance in the commercial campus. The detailed explanations of notations are provided in the Appendix.

2.2.1.1 HVAC

The indoor temperature of a CB is one of the most important features to evaluate the comprehensive comfort levels of its occupants, where the relationship between the power consumed by the HVAC system and the indoor temperature can be represented by the following constraints:

$$T_{t+1}^{\text{hvac}} = \beta^{\text{hvac}} T_t^{\text{hvac}} + \alpha^{\text{hvac}} U_t, \forall t, \tag{2.1}$$

where $T_t^{\text{hvac}} = [T_t^{\text{in}}, T_t^{\text{iw}}, T_t^{\text{ow}}]^T$, including the indoor temperature, inner wall temperature, and outer wall temperature, respectively. $U_t = [T_t^{\text{out}}, \Psi_t, \sigma_t \eta\, p_t^{\text{hvac}}]^T$, including the outdoor temperature, solar irradiance, binary on/off action indicator of the HVAC system, and constant power consumption of the HVAC system, respectively. α and β are the environment coefficients of the CB [29].

$$T_d^{\text{hvac}} - \delta^{\text{hvac}} \leq T_t^{\text{in}} \leq T_d^{\text{hvac}} + \delta^{\text{hvac}}, \forall t, \tag{2.2}$$

where T_d^{hvac} is the desired indoor temperature and δ^{hvac} is the maximum deviation from the desired indoor temperature.

Moreover, consumers' comfort level can be related to an HVAC system as follows:

$$J_{\text{hvac},t} = \begin{cases} 0, & T_t^{\text{in}} \geq T^{\max} \\ 1 - \frac{T_t^{\text{in}} - (T_d^{\text{hvac}} + \varepsilon^{\text{hvac}})}{\delta^{\text{hvac}}}, & T_d^{\text{hvac}} + \varepsilon^{\text{hvac}} \leq T_t^{\text{in}} \leq T^{\max} \\ 1, & T_d^{\text{hvac}} - \varepsilon^{\text{hvac}} \leq T_t^{\text{in}} \leq T_d + \varepsilon^{\text{hvac}} \\ \frac{T_t^{\text{in}} - (T_d^{\text{hvac}} - \delta^{\text{hvac}})}{\delta^{\text{hvac}}}, & T^{\min} \leq T_t^{\text{in}} \leq T_d^{\text{hvac}} - \varepsilon^{\text{hvac}} \\ 0, & T_t^{\text{in}} \leq T^{\min}. \end{cases} \tag{2.3}$$

The comfort indoor temperature zone is defined as $T_d^{\text{hvac}} \pm \varepsilon^{\text{hvac}}$, where $\varepsilon^{\text{hvac}}$ is the maximum deviation from the desired indoor temperature that can still ensure a comfort temperature zone.

2.2.1.2 EWH

The hot water demand within the CB is supported by the EWH, such that the requirements for the EWH can be expressed as follows:

$$T_\tau^{\text{ewh}} = T_0^{\text{ewh}} + \Delta T^{\text{ewh}}, \Delta T^{\text{ewh}} = \sum_{t=1}^{\tau} \frac{\zeta^{\text{ewh}} z_t^{\text{ewh}} p_t^{\text{ewh}} - H_t^{\text{de}}}{C_{\text{water}} M}, \forall \tau, \tag{2.4}$$

where p_t^{ewh} is the constant power consumption of the EWH. Binary variable z_t^{ewh} denotes the on/off action indicator of the EWH. ζ^{ewh} is the power-to-heat ratio of the EWH. Auxiliary state variable ΔT^{ewh} is the temperature deviation of the EWH between the beginning of the operating day and time τ. Parameter H_t^{de} represents the aggregated negative impacts on the temperature of the hot water in the EWH, including heat loss that is transferred to its ambient, outflow of hot water and inflow of cold water. Parameter M is the mass of the water in the hot water tank, and C_{water} is the specific heat capacity of water.

Moreover, the water temperature in the EWH is closely related to the occupants' comfort level,

so it is relatively important to maintain this temperature above a certain threshold.

$$T_d^{\text{ewh}} - \delta^{\text{ewh}} \leq T_\tau^{\text{ewh}}, \forall \tau \tag{2.5}$$

Parameter T_d^{ewh} is the desired water temperature in the hot water tank of the EWH.

$$J_{\text{ewh},\tau} = \begin{cases} 1, & T_d^{\text{ewh}} \leq T_\tau^{\text{ewh}} \\ \frac{T_\tau^{\text{ewh}} - (T_d^{\text{ewh}} - \delta^{\text{ewh}})}{T_d^{\text{ewh}} - (T_d^{\text{ewh}} - \delta^{\text{ewh}})}, & T_d^{\text{ewh}} - \delta^{\text{ewh}} \leq T_\tau^{\text{ewh}} \leq T_d^{\text{ewh}} \\ 0, & T_\tau^{\text{ewh}} \leq T_d^{\text{ewh}} - \delta^{\text{ewh}}. \end{cases} \tag{2.6}$$

Parameter δ^{ewh} is the maximum allowed deviation from the desired water temperature.

2.2.1.3 PEV

Additionally, we have the following charging dynamics for PEVs:

$$SoC_{v,t} = SoC_{v,t-1} + \frac{p_{v,t}^{\text{ch}} \eta_v^{\text{ch}} I_{v,t} u_{v,t}^{\text{ch}}}{\overline{E}_v}, \forall v, t, \tag{2.7}$$

where $p_{v,t}^{\text{ch}}$ is the constant charging rate of the v-th PEV. Parameter η_v^{ch} is the charging efficiency of the v-th PEV. Parameter $\overline{E}_v$ is the rated energy of the v-th PEV. We use a binary variable $u_{v,t}^{\text{ch}}$ to represent charging decisions, i.e., if $u_{v,t}^{\text{ch}}$ is 1, the v-th PEV is being charged; when $u_{v,t}^{\text{ch}}$ is 0, the v-th PEV is in an idle status. Also, seeing as the arrival and departure schedules of each PEV are uncertain, we adopt a binary parameter $I_{v,t}$ to model the location of each PEV, such that, where $I_{v,t} = 1$ when the PEV is ready for the charging process and $I_{v,t} = 0$ when the PEV is not in the parking lot.

In addition, the SoC of each PEV must be maintained within a certain range as follows:

$$\underline{SoC}_v \leq SoC_{v,t} \leq \overline{SoC}_v, \forall v, t, \tag{2.8}$$

where upper bound $\overline{SoC}_v$ and lower bound $\underline{SoC}_v$ are defined.

Furthermore, the comfort level related to the v-th PEV can be defined as follows:

$$J_{v,t} = \begin{cases} 1, & SoC_v^d \leq SoC_{v,t} \\ \frac{SoC_{v,t} - SoC_v^{\text{base}}}{SoC_v^d - SoC_v^{\text{base}}}, & SoC_v^{\text{base}} \leq SoC_{v,t} \leq SoC_v^d \\ 0, & SoC_{v,t} \leq SoC_v^{\text{base}}. \end{cases} \tag{2.9}$$

$J_{v,t}$ denotes the comfort level of the v-th PEV owner. SoC_v^d is the desired SoC for the v-th PEV.

SoC_v^{base} represents the base SoC required for the v-th PEV with a round trip between the owner's house and the CB.

2.2.1.4 ESS

Similarly, we have the following charging and discharging dynamics for ESSs:

$$SoC_{k,t} = SoC_{k,t-1} + \frac{p_{k,t}^{\text{ch}} \eta_k^{\text{ch}} u_{k,t}^{\text{ch}} - \frac{p_{k,t}^{\text{dis}} u_{k,t}^{\text{dis}}}{\eta_k^{\text{dis}}}}{\overline{E}_k}, \forall k, t, \tag{2.10}$$

where $p_{k,t}^{\text{ch}}$ and $p_{k,t}^{\text{dis}}$ are the constant power charged into or discharged from the k-th ESS at time t, and η_k^{ch} and η_k^{dis} represent the charging and discharging efficiencies of the k-th ESS, respectively. $u_{k,t}^{\text{ch}}$ and $u_{k,t}^{\text{dis}}$ are binary variables indicating charging and discharging decisions of the k-th ESS.

Parameter $\overline{E}_k$ denotes the rated energy level of the k-th ESS. Each ESS has a finite capacity; therefore, energy stored in each one must have the following lower and upper bounds:

$$\underline{SoC}_k \leq SoC_{k,t} \leq \overline{SoC}_k, SoC_{k,0} = SoC_{k,T}, \forall k, t, \tag{2.11}$$

where $\overline{SoC}_k$ is the upper bound and $\underline{SoC}_k$ is the lower bound of the k-th ESS' SoC status. Moreover, we set the initial available SoC to be the same as the final available SoC for a better scheduling of peak hours for each operating day.

ES units have charging and discharging limits as follows:

$$0 \leq u_{k,t}^{\text{ch}} + u_{k,t}^{\text{dis}} \leq 1, \forall k, t, \tag{2.12}$$

where the k-th ESS cannot be charged and discharged at the same time.

2.2.1.5 CHP

In order to provide sufficient electricity to the CB in both the islanded mode and the grid-connected mode, gas-based combined heat and power (CHP) is deployed. Without loss of generality, we assume the CHP unit has been off for enough time prior to the operating day. We first formulate the upper/lower limit on the power output of the CHP as follows:

$$\underline{P}_c I_{c,t} \leq p_{c,t} \leq \overline{P}_c I_{c,t}, \forall c, t. \tag{2.13}$$

Note that when CHP c is off, i.e., $I_{c,t} = 0$, the power output of CHP c must be 0.

Additionally, the increase and decrease of the CHP power outputs between two consecutive time slots are constrained by ramping-up and ramping-down rates, as well as by power output

limits. When c is started up at time t, i.e., $y_{c,t} = 1$, it can generate at most $\overline{SU}_c$ in time slot t. The ramping-down case is modeled similarly. Therefore, we have the following ramping-up and ramping-down constraints for the CHP:

$$\begin{aligned} &p_{c,t} - p_{c,t-1} \leq \mathrm{RU}_c I_{c,t-1} + \overline{P}_c(1 - I_{c,t}) + \overline{SU}_c y_{c,t}, \forall c, t \\ &p_{c,t-1} - p_{c,t} \leq \mathrm{RD}_c I_{c,t} + \overline{P}_c(1 - I_{c,t-1}) + \overline{SD}_c z_{c,t}, \forall c, t. \end{aligned} \tag{2.14}$$

In addition, for each c, we have the following minimum up/down time constraints:

$$\sum_{\tau=t}^{t+\mathrm{UT}_c-1} I_{c,\tau} \geq \mathrm{UT}_c y_{c,t}, \quad \sum_{\tau=t}^{t+\mathrm{DT}_c-1} (1 - I_{c,\tau}) \geq \mathrm{DT}_c z_{c,t}, \forall c, t. \tag{2.15}$$

The relationship between startup and shutdown action decisions $y_{c,t}$ and $z_{c,t}$ of c is given as follows:

$$I_{c,t} - I_{c,t-1} = y_{c,t} - z_{c,t},\ y_{c,t} + z_{c,t} \leq 1, \forall c, t. \tag{2.16}$$

2.2.2 Reliability Constraints

2.2.2.1 Uncertain Grid-connection Conditions

We also use $\overline{P}$ to represent the capacity limit on the point of common coupling (PCC). As described in the introduction, the uncertain grid-connection condition is one of the key uncertainties that needs to be considered in the proactive resilient scheduling problem. The power exchange through the PCC between the CB and the main grid is zero during the extreme event. Thus, the parameter $I_{g,t} \in [0, 1]$ is adopted to model the uncertain grid-connection condition. Thus, we have the following constraints on the grid-connected tie-line:

$$\begin{aligned} &0 \leq p_{g,t} u_{g,t} \leq \overline{P}_g I_{g,t}, \forall g, t \\ &\sum_g u_{g,t} \leq 1, \forall t. \end{aligned} \tag{2.17}$$

Parameter $p_{g,t}$ represent real-time power buy from a retail electricity market. Binary variable $u_{g,t}$ is proposed to model the power purchasing decision.

2.2.2.2 Power Balance

Furthermore, we denote aggregate critical power loads as d_t that must be satisfied [30]. Therefore, we have following power balance equation:

$$\begin{aligned}&\sum_k \left(p_{k,t}^{\mathrm{dis}} u_{k,t}^{\mathrm{dis}} - p_{k,t}^{\mathrm{ch}} u_{k,t}^{\mathrm{ch}}\right) + w_t + p_{g,t} u_{g,t} + \sum_c p_{c,t} I_{c,t} \\ =&l_t + d_t + p_t^{\mathrm{ewh}} z_t^{\mathrm{ewh}} + p_t^{\mathrm{hvac}} \sigma_t + \sum_v p_{v,t}^{\mathrm{ch}} I_{v,t} u_{v,t}^{\mathrm{ch}}, \forall t.\end{aligned} \tag{2.18}$$

Parameter w_t denotes the output of renewables. Variable l_t represents the power mismatch due to the unexpected extreme weather event.

2.2.3 Proactive Resilient Reserves

In order to provide optimal scheduling decisions to ensure the resilience of the commercial campus, the CHP and ESSs need to satisfy the minimum reserve requirement to maintain the resilience of the CB [25]. In our proposed model, the resilience of the CB needs to be guaranteed for the entire operating day. Therefore, the minimum requirement for the energy reserve is to compensate for any insufficiencies during the extreme weather event. Variable $P_{re,t}^{+}$ is introduced as reserves that must be satisfied when power scheduled to be bought from the retail electricity market cannot be delivered due to the extreme weather event. Ramping-up of the CHP $p_{c,t}^{RU}$ and power discharging of ESSs $p_{k,t}^{re,\mathrm{dis}}$ are major contributions to the power reserve $P_{re,t}^{+}$.

The constraints related to the islanding capability based reserve can be expressed by the following formulation:

$$P_{re,t}^{+} = \sum_c p_{c,t}^{RU} + \sum_k p_{k,t}^{re,\mathrm{dis}}, \forall t. \tag{2.19}$$

In addition, the relationship between the proactive resilient reserve and the power exchange schedule can be formulated as follows:

$$\overline{P}_g \geq P_{re,t}^{+} \geq p_{g,t}, \forall t. \tag{2.20}$$

Furthermore, for each aforementioned component, the reserves for the optimal proactive resilient scheduling strategy have the following upper/lower bounds:

$$\begin{aligned}&p_{c,t}^{RU} \leq \mathrm{RU}_c I_{c,t-1} + \overline{P}_c (1 - I_{c,t}) + \overline{SU}_c y_{c,t}, p_{c,t}^{RU} \leq \overline{P}_c I_{c,t} - p_{c,t}, \forall c, t \\ &p_{k,t}^{re,\mathrm{dis}} \leq p_k^{\mathrm{dis}} u_{k,t}^{\mathrm{dis}}, \ \frac{p_{k,t}^{re,\mathrm{dis}}}{\eta_k^{\mathrm{dis}}} \leq SoC_{k,t} \overline{E}_k - \underline{E}_k, \forall k, t.\end{aligned} \tag{2.21}$$

Parameter $\underline{E}_k$ denotes the minimum allowed energy level of the k-th ESS.

2.3 Safe Reinforcement Learning

In this section, our objective is to develop an optimal proactive resilient scheduling strategy for the central controller of a CB that can minimize the costs from a potential extreme weather event and maximize comprehensive comfort levels for occupants during office hours (from 8:00 am to 8:00 pm). As mentioned in the introduction section, grid-connected conditions, power generation of rooftop solar panels, intermittent load demand in the CB, arrival state-of-charges (SoCs), and arrival/departure time of PEVs, are major uncertainties associated with the extreme weather event that need to be considered in the training process, especially for the extreme epochs. In order to mitigate the influence of lack of comprehensive information on the distribution of certain uncertainties, we model the proactive resilient scheduling of the CB as a Markov decision process (MDP) [31], with the environment models formulated as in previous sections at each time step t.

In addition, we formulate the MDP model based on a tuple with four vectors: $\mathbb{S}$, $\mathbb{A}$, $\mathbb{R}$, $\mathbb{S}'$, where $\mathbb{S}$ and $\mathbb{A}$ denote the state and action spaces, respectively. $\mathbb{S}'$ is the state space after the transition through the environment from the original state space $\mathbb{S}$, i.e., from time t to time $t+1$. $\mathbb{R}: \mathbb{S} \times \mathbb{A} \times \mathbb{S}' \Rightarrow R$ represents the reward function, i.e., the immediate reward obtained by the central controller of the CB after taking action A, which changes the state space from S to S'. In the proposed model, the states are considered to be continuous for the whole time interval, while the actions are said to be discrete, which adheres to the nature of the major components in a CB that require simple actions, such as the on/off actions of an ESS.

Moreover, risks associated with the extreme weather uncertainties need to be tackled during the training process in order to mitigate the influence caused by potential extreme epochs. Thus, an SRL algorithm has been developed by combining the DQN method and CVaR method considering all the unique features of the proactive resilient scheduling problem.

2.3.1 DQN Based Resilient Proactive Scheduling

The detailed information for the state space, action space, and reward function of the proposed DQN is introduced as follows:

States: The major states of the SRL based proactive scheduling strategy are represented by vector $\mathbb{S}$, including $[T_t^{\text{in}}, SoC_{v,t}, SoC_{k,t}, T_\tau^{\text{ewh}}, p_{c,t}, p_{g,t}, l_t]$, which indicate the indoor temperature, the SoC of PEV v, the SoC of ESS k, the water temperature of the EWH, the power generation of the CHP c, power buying from the main grid, and the power mismatch, respectively.

Actions: The actions of the SRL based proactive scheduling strategy are represented by vector

$\mathbb{A}$, including $[\sigma_t,\ u_{v,t}^{\text{ch}},\ (u_{k,t}^{\text{ch}},\ u_{k,t}^{\text{dis}}),\ z_t^{\text{ewh}},\ u_{g,t},\ y_{c,t},\ z_{c,t}]$. The on/off status of the HVAC system, the charging/idle status of the PEVs, the charging/discharging status of the ESS, the load serving condition of the EWHs, the binary variable that selects which power amount to buy from the main grid, and the unit commitment decisions of the CHPs are considered in action space $\mathbb{A}$. All action variables are binary variables, which adhere to the nature of the major components in a CB.

Reward: Our objective is to minimize damage caused by the extreme weather event while maximizing occupants' comfort levels for the central controller of the CB, where risks associated with the proactive scheduling process are managed through CVaR. Thus, we formulate the reward of the proactive scheduling problem as follows:

$$\begin{aligned} R = &-\sum_t C_{\text{g}} p_{g,t} u_{g,t} - \sum_t \sum_k C_{\text{ESS}} (p_{k,t}^{\text{ch}} u_{k,t}^{\text{ch}} + p_{k,t}^{\text{dis}} u_{k,t}^{\text{dis}}) - \sum_t \sum_c C_{\text{gas}} p_{c,t} - \sum_t C_p |l_t| \\ &+ \sum_t J_{\text{hvac},t} + \sum_{t=72}^{80} \sum_v J_{v,t} + \sum_t J_{\text{ewh},t}. \end{aligned} \tag{2.22}$$

Note that C_{g} denotes the real-time electricity price. Parameter C_{ESS} is the degradation cost coefficient of the ESS. Parameter C_{gas} represents the gas price. Parameter C_p is the penalty cost when a power mismatch occurs.

2.3.2 CVaR

In the proposed SRL approach, the reward of each epoch is a random variable that involves the aforementioned uncertainties. In the reward distribution, there are optimal proactive resilient scheduling strategies with negative rewards (which are huge penalties) for the worst-case epochs that have rather small possibilities to occur. Therefore, a risk aversion approach is needed to avoid such an issue, which can ensure that the penalty variability is minimized as desired. In our model, the variability among the rewards of all epochs is handled by a CVaR method. In the CVaR method, the risk of the proposed problem is minimized through minimizing epochs with penalties larger than the $(1-\varepsilon)$–quantile of the reward distribution, i.e., the value-at-risk (VaR) ζ, where ε is the confidence level [32]. The relationship between the VaR and the rewards can be represented through the following constraints:

$$\varepsilon \geq \text{R}^e - \zeta, \varepsilon \geq 0. \tag{2.23}$$

In the proposed model, we use R^e to represent the reward of epoch e. Non-negative auxiliary variable ε denotes the deviation between the reward and the VaR. Therefore, the training process is utilized to select the proper action pairs, where the influence from extreme epochs in the learning process can be mitigated.

2.3.3 Procedure to Merge DQN and CVaR

An SRL control approach is designed based on unsupervised DQN and CVaR methods to provide proactive resilient scheduling decisions for a CB, which minimizes the damage caused by an extreme weather event while maximizing comfort levels of occupants in the CB. Detailed information on the proposed SRL method regarding the combination of DQN and CVaR can be found in the following Fig. 2.3:

Algorithm 1 Safe Reinforcement Learning

function MERGE DQN AND CVAR($\mathbb{S}$, $\mathbb{A}$, $\mathbb{R}$, $\mathbb{S}'$)
  Inputs $\leftarrow$ States:T_t^{in}, $SoC_{v,t}$, $SoC_{k,t}$, T_τ^{ewh}, $p_{c,t}$, $p_{g,t}$, l_t
  Outputs $\rightarrow$ Actions:σ_t, $u_{v,t}^{\text{ch}}$, $u_{k,t}^{\text{ch}}$, $u_{k,t}^{\text{dis}}$, z_t^{ewh}, $u_{g,t}$, $y_{c,t}$, $z_{c,t}$
  Initialize Parameters for the Environment
  Initialize Memories for the SRL
  for $e = 1$ to E **do**
    Reset the environment, and obtain the state $\mathbb{S}_0$
    for $t = 1$ to T **do**
      Obtain the state-action pairs through DQN
      Update the state-action pairs through CVaR
      Store state-action pairs, update reward distribution
      if memory counter $\geq$ batch memory size **then**
        Repeat, update parameters of the DQN, such as ϵ-greedy
      end if
    end for
    Store rewards, losses and update batch epoches
  end for
end function

Figure 2.3: The process of merging DQN and CVaR.

2.4 Simulation Results

In this section, the proposed algorithm is evaluated through real-world data sets. First, the selected real-world data sets are described in detail. Then, the performance of the proposed DRL algorithm is evaluated. All simulations are implemented on a desktop computer with a 3.0 GHz Intel Core i5-7400 CPU and 8GB RAM. The proposed DRL based energy management problem is simulated using Python 3.5, Gurobi 8.0, and Tensorflow 1.8.

2.4.1 Numerical Settings

The proposed system is tested in a commercial campus with a CB, two charging piles for PEVs, and three CHPs. In the CB, there is one HVAC system, two EWHs, two ESSs, one pack

Table 2.1: Comfort Level Related Parameters

Type	T_d^{hvac} ($^\circ C$)	δ^{hvac} ($^\circ C$)	$\varepsilon^{\text{hvac}}$ ($^\circ C$)
HVAC	23	5	1
Type	E_k^d (%)	E_k^{base} (%)	E_k^0 (%)
PEV	80	10	10
Type	T_d^{ewh} ($^\circ C$)	δ^{ewh} ($^\circ C$)	T_0^{ewh} ($^\circ C$)
EWH	40	10	30

Table 2.2: ESS Parameters

$\underline{SoC}_k$ (%)	$\overline{SoC}_k$ (%)	$p_{k,t}^{\text{ch}}$ (kW)	$p_{k,t}^{\text{dis}}$ (kW)
10	90	15	15

Table 2.3: PEV Parameters

Type	$\underline{SoC}_v$ (%)	$\overline{SoC}_v$ (%)	$p_{v,t}^{\text{ch}}$ (kW)
Tesla Model S 75D	20	90	11.5
Tesla Model X 100D	20	90	17.2
Nissan Leaf SV	20	90	3.6

Table 2.4: CHP Parameters

Unit	UT_c (hr)	DT_c (hr)	$\underline{P}_c$ (kW)	$\overline{P}_c$ (kW)
1	0.25	0.25	47.5	594.2
2	0.25	0.25	29.8	373.4
3	0.25	0.25	15.4	294.5
Unit	RU_c (kW)	RD_c (kW)	$\overline{SU}_c$ (kW)	$\overline{SD}_c$ (kW)
1	109.8	109.8	297.1	475.4
2	74.7	74.7	186.7	298.72
3	58.9	58.9	147.3	235.6

of rooftop solar panels, and one base load. All parameters are unified for computational proposes, with P_{base} set at $1,867kW$ and H_{base} set at $1,224kBtu$. Comfort levels are only considered during business hours, when occupants are in the CB (from 8 a.m. to 8 p.m.). The parameters related to the occupants' comfort levels are shown in Table 2.1.

The ESSs have an identical storage capacity of 80 kWh, and have a charging and discharging efficiency of 0.98. Other parameters regarding the ESSs are listed in Table 2.2. To prolong the ESSs' lifetime, their SoCs should not drop below 10% or be overcharged above 90%. Both the initial and final SoCs of the ESSs are set to be 50%. Degradation cost coefficient C_{ESS} of each ESS is set to be $0.0035\$/kWh$. The arrival and departure time of the PEVs is randomly sampled within 8:00 am–9:00 am and 6:00 pm–8:00 pm following a normal distribution, and the arrival SoCs are generated following a normal distribution with a mean of 30% SoC and a variance of 10% SoC. The types of PEVs and their parameters are listed in Table 2.3. Parameters η, α^{hvac},

β^{hvac}, and p_t^{hvac} of the HVAC system are from [33]. The data for the EWHs is from [34]. The EWHs' power to heat ratio is set to 1.2. Moreover, the total capacity of the installed solar panels is 60 kW, where the historic generation patterns are from [35], with proper scaling coefficients. The historical data of the solar irradiance and the outdoor temperature is from [36], with proper scaling coefficients. The data for the base load and the hot water demand is from [37]. The penalty for the power mismatch is from [38]. The parameters for the CHPs are presented in Table 2.4, where the gas price for the CHPs is 0.013 $\$/kW$.

The TOU electricity price is obtained from the real-world wholesale electricity prices of PJM [39], with proper scaling coefficients. The uncertain grid-connection condition $I_{g,t}$ follows a Bernoulli distribution.

2.4.2 Case Study

The case study is conducted through four steps: (i) show the convergence rate of the proposed SRL algorithm in handling such complicate environment; (ii) compare the proposed SRL algorithm with a DRL algorithm in both training and testing processes to show the effectiveness of utilizing CVaR with DQN; (iii) compare the proposed SRL algorithm with a scenario-based stochastic programming and a CVaR-based stochastic optimization approach to show the optimality of the proposed SRL algorithm and the importance of considering risks through the CVaR method; and (iv) select one extreme epoch in the testing process to show the resilience of the commercial campus when facing an extreme event with the proactive scheduling strategy.

2.4.2.1 SRL versus DRL

We first train the proposed SRL based proactive resilient scheduling problem with 10000 highly intermittent episodes that are generated based on four uncertainties: grid-connection conditions, base load demand, power output of renewables, and PEV arrival SoC and arrival/departure time. As shown in Fig. 2.4, the smoothed rewards for the operating day increases as the number of training episodes increases. Even though the rewards tend to vary during the training process due to the uncertainties, the proposed SRL learns the optimal action pairs quickly. Moreover, as shown in Fig. 2.5, the smoothed losses for the operating day decreases as the number of training episodes increases. The red dotted line shows the trend of the losses. This result demonstrates that the randomly selected samples are closer to the batch episodes.

In addition, we compare the proposed SRL algorithm with deep reinforcement learning (DRL), which is the combination of DQN and RL in both the training and testing processes, keeping states, actions, environment, and reward function are the same.

As shown in Fig. 2.6 and Fig. 2.7, the DRL algorithm is also trained with the same 10000

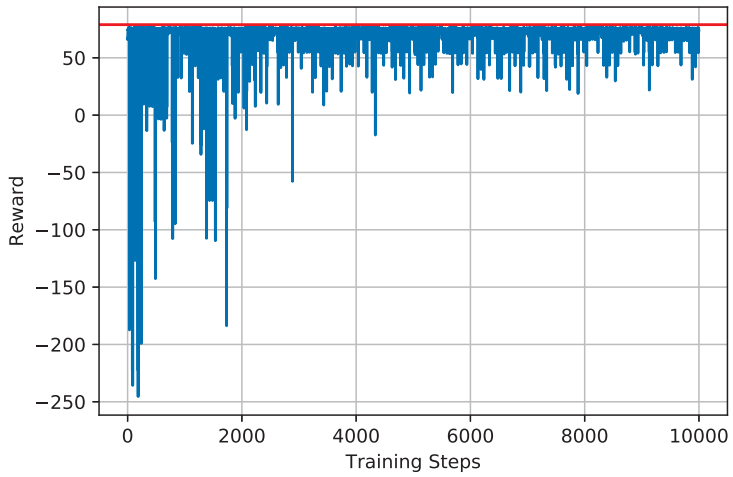

Figure 2.4: The reward of the proposed SRL algorithm in the training process under 10000 highly intermittent episodes.

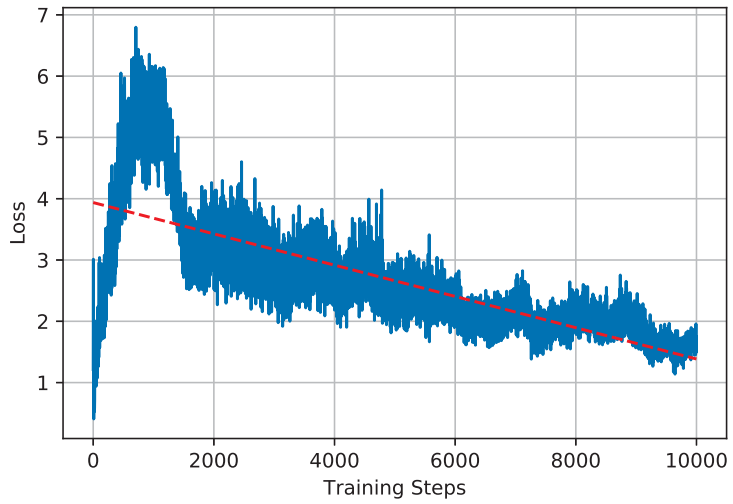

Figure 2.5: The loss of the proposed SRL algorithm in the training process under 10000 highly intermittent episodes.

episodes that are generated with the aforementioned uncertainties. During the training process, the convergence of the DRL algorithm is faster than that of the proposed SRL algorithm and the losses of the DRL are also lower than those of the proposed SRL method. The reason why the SRL algorithm converges slower than the DRL algorithm is that the proposed SRL algorithm eliminates the extreme epochs during the training process, which requires more steps to converge. Doing so can also help the DQN's training process in handling various uncertainties in the real-world test cases, especially to avoid the extreme epoch shown in Fig. 2.6. Also, the training process of the proposed SRL algorithm takes 6 hours which is only a little more than that of the DRL algorithm,

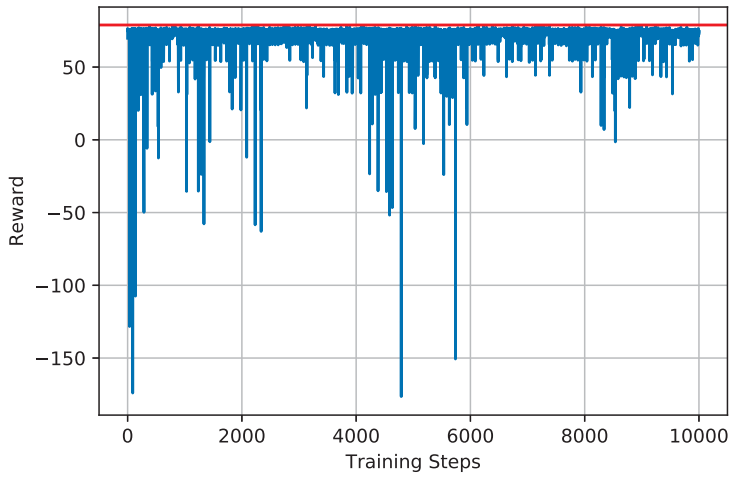

Figure 2.6: The reward for the DRL method in the training process under the same 10000 highly intermittent episodes.

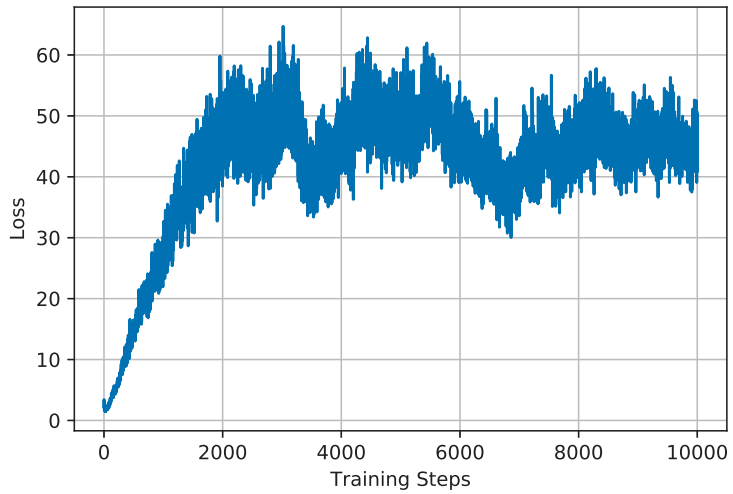

Figure 2.7: The loss for the DRL method in the training process under the same 10000 highly intermittent episodes.

which is acceptable.

After comparing the training process of the proposed SRL algorithm and the DRL method, we test the two trained DQNs with an identical 1000 totally new episodes generated from different uncertainty distributions.

The rewards of the SRL algorithm and of the DRL method based on these new episodes are presented in Fig. 2.8 and Fig. 2.9. As we can observe from Fig. 2.8, the rewards of the SRL based method are higher than those of the DRL based method. Moreover, the rewards of the SRL based method are much smoother than those of the DRL based method. This is because, through the

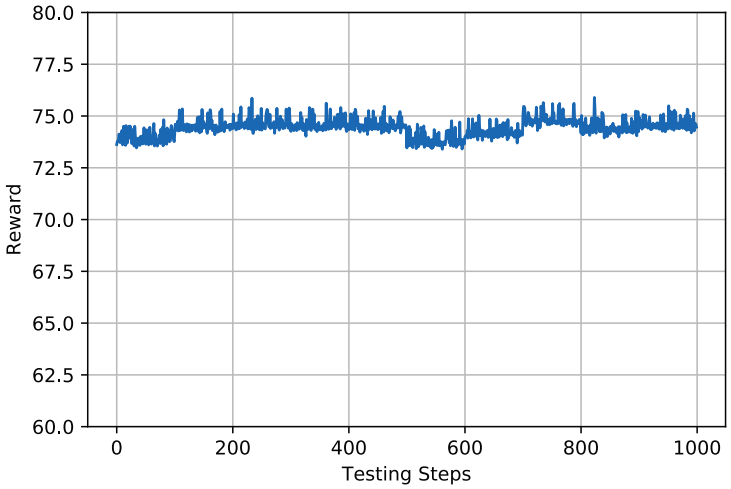

Figure 2.8: The reward of the proposed SRL algorithm when testing under 1000 new episodes containing various extreme conditions.

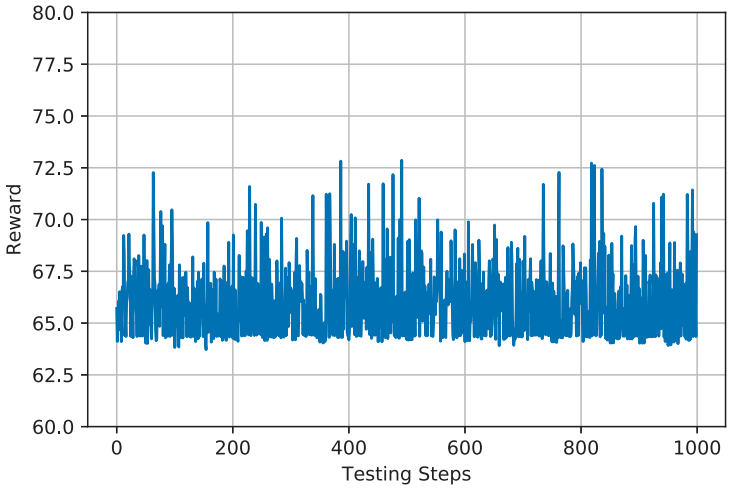

Figure 2.9: The reward of the DRL method when testing under 1000 new episodes containing various extreme conditions.

training process, the proposed SRL method has the capability to handle extreme conditions, while the DRL method does not.

2.4.2.2 SRL versus Scenario-based Stochastic Programming

To benchmark the optimality of the proposed SRL approach, we adopt a scenario-based stochastic optimization approach to provide resilient control decisions for the central controller of the CB based on the same 10000 scenarios generated from the four uncertainties. The probability of each scenario is assumed to be $1/10000$. The objective function for the scenario-based stochas-

tic approach is the same as the reward function for the proposed SRL. Through Python and Gurobi, we attain the expected value of the objective function as 77.62 (represented as the red line) for the operating day, which validates the convergence of the proposed SRL approach after the training process, as shown in Fig. 2.4. However, compared to the 6 hours of training required for SRL based proactive scheduling to converge, the scenario-based stochastic programming method takes much longer, needing 28 hours to converge (note that this is when the scenario reduction process is not considered). Furthermore, when applying CVaR with the selected scenario-based stochastic optimization approach, which becomes a risk-constrained stochastic programming problem, the performance when facing an extreme weather event is also better than when using the original stochastic programming method, which results in an expected objective of 78.53 with the 10000 scenarios. This is because, with the help of CVaR, the worst-case scenarios have been eliminated by the risk averse decisions.

2.4.2.3 Sensitivity Analysis

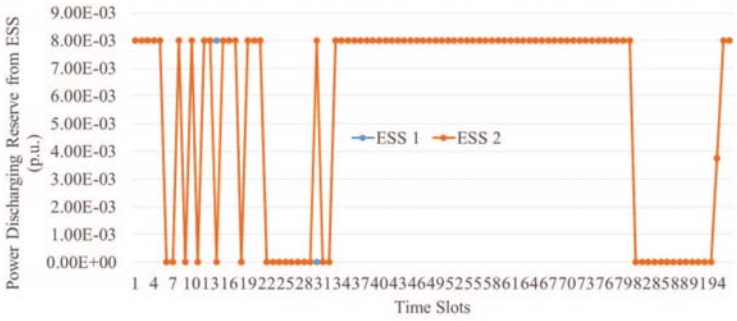

Figure 2.10: The power discharging reserve from ESSs in per unit value.

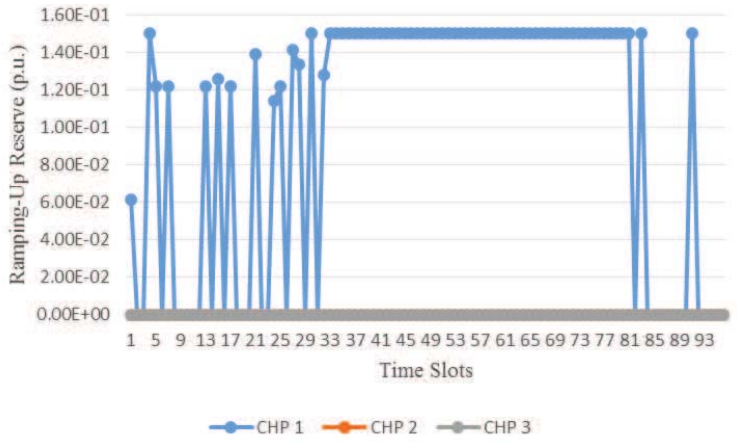

Figure 2.11: The ramping-up reserve from CHPs in per unit value.

In addition, we test the resilience of the proposed framework, utilizing both the proactive scheduling strategy and CDR under various extreme epochs to show the effectiveness of the SRL in considering both the exploration and exploitation. The extreme weather event is set to occur at the 44th time slot, and its total islanding period is two hours, during which time no power can be exchanged through the PCC. As shown in Fig. 2.10 and Fig. 2.11, the reserve for the power mismatch is provided by two major components in the commercial campus: CHPs and ESSs. Specifically, the ramping-up reserve from CHPs and the power discharging reserve from ESSs contribute to the resilience of the CB. The extreme weather event occurs at the 44th time slot during business hour, where the real-time power buying from the retail electricity market is zero until the 52nd time slot. During the islanding period, the shorted power is supported by the reserves from CHPs and ESSs, which increase the operating costs slightly but enhance the resilience of the commercial campus.

2.4.2.4 Scalability of the Proposed Proactive Resilient Scheduling Strategy

Then we extend the proposed system modeling to multiple CBs to show the effectiveness and scalability of the proposed proactive resilient scheduling strategy.

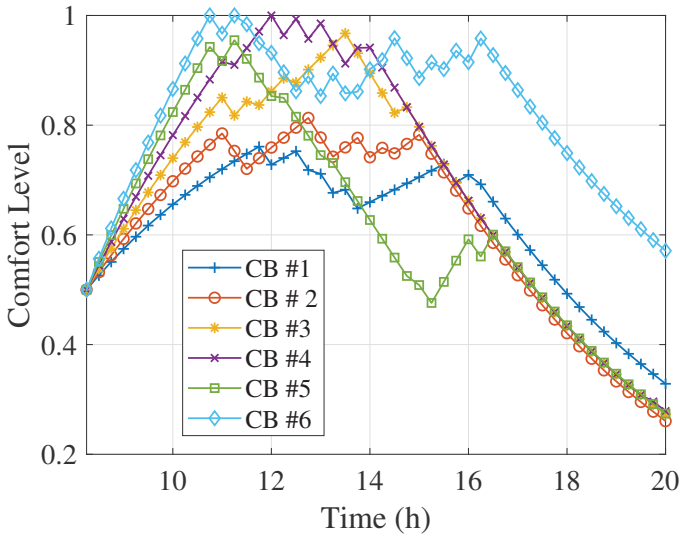

Figure 2.12: Comfort level related to the indoor temperature of CBs.

The second-stage (real-time) decisions are generated based on the first-stage (day-ahead) decisions after the uncertainties are unveiled in one selected scenario from the $1,000,000$ original scenarios. The unit commitment decisions as well as the buying/selling amount scheduled in the day-ahead retail electricity market cannot be changed throughout the operating day. As considered in the problem formulation section, we need to consider both the comfort levels of the occupants

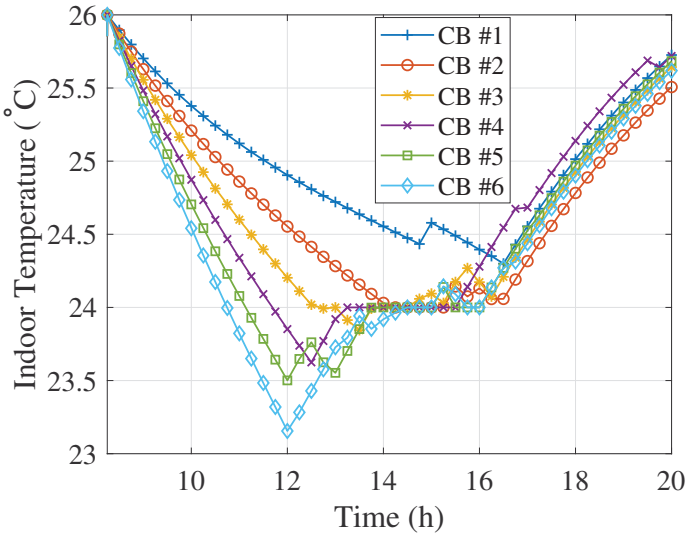

Figure 2.13: Indoor temperature of CBs.

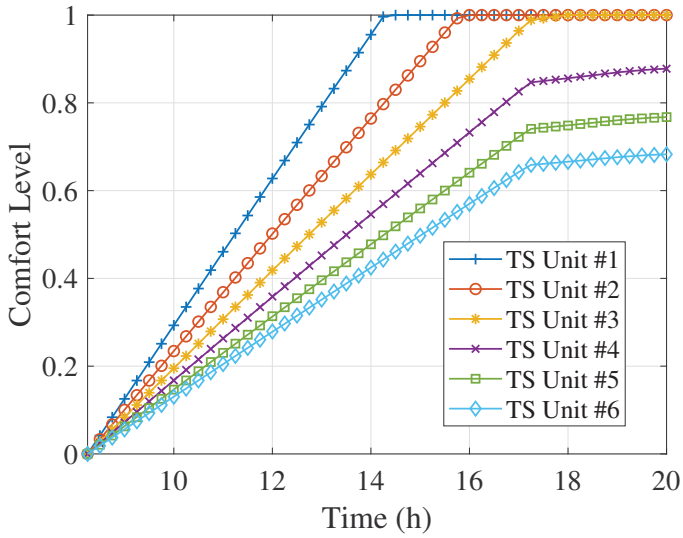

Figure 2.14: Comfort level related to water temperature in TS units.

and the reliability of the commercial campus. We first show the comprehensive comfort levels in Fig. 2.12, Fig. 2.14, and Fig. 2.16 to validate the effectiveness of the proposed energy management strategy in handling both the O&M costs and the comprehensive comfort levels. As shown in Fig. 2.13, even though the comfort level related to HVAC systems cannot remain in the most comfort level zone during the entire business hours, the indoor temperatures of all CBs still remain in the pre-defined temperature tolerance in Table 2.1. Since the comfort level related to PEVs only regards to the SoCs when departure as shown in Fig. 2.17, therefore, it has more priority during

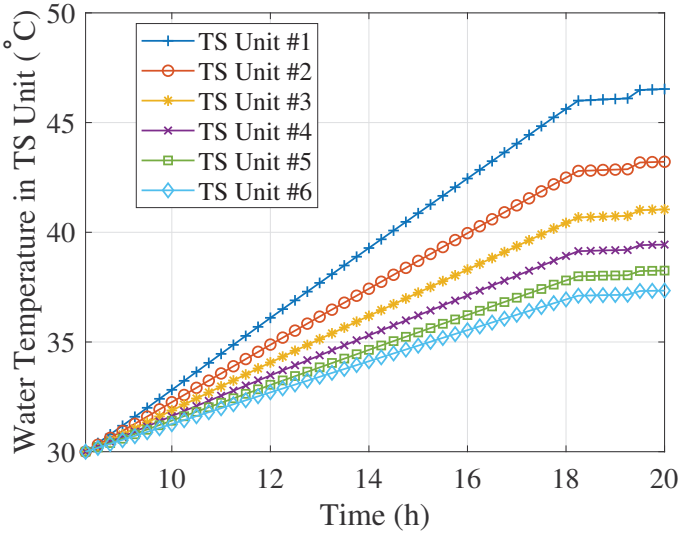

Figure 2.15: Water temperature in TS units.

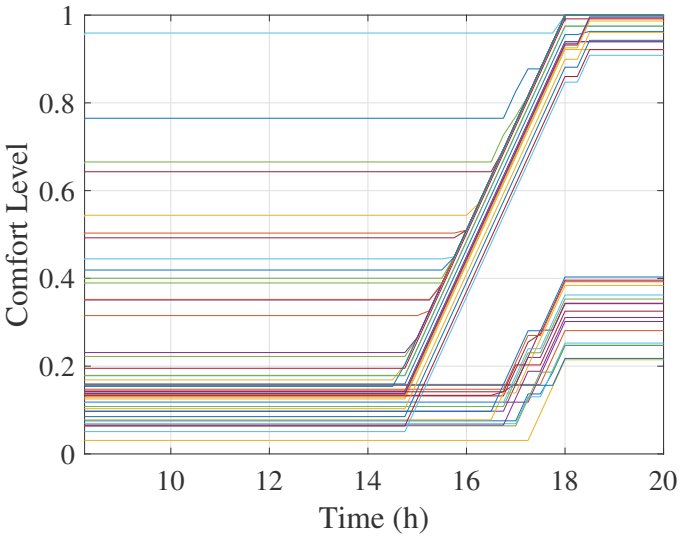

Figure 2.16: Comfort level related to SoCs of PEVs.

that period than the HVAC system which depends on the whole business hours. In addition, the water temperature in TS units are also provided in Fig. 2.15. By utilizing heat boilers, EWHs, and CHP units, the TS units can ensure the comfort level related with the water temperature never drop.

2.4.2.5 Islanding Capability with/without Reserves

In addition to the scalability, we compared the proposed resilient proactive scheduling strategy with and without using the islanding capability based reserve method in the same uncertain grid-

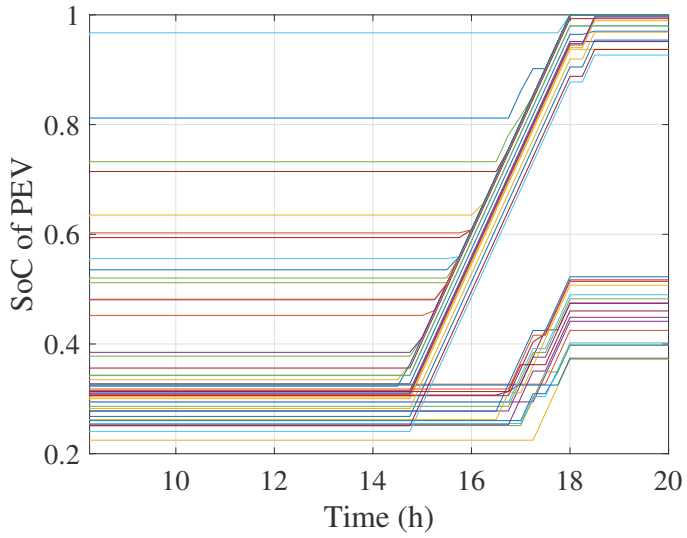

Figure 2.17: SoCs of PEVs.

connection situation, where all other system settings remain the same. The islanding issue is set to occur at the 44-th time slot, where no power can be exchanged through the PCC at that time.

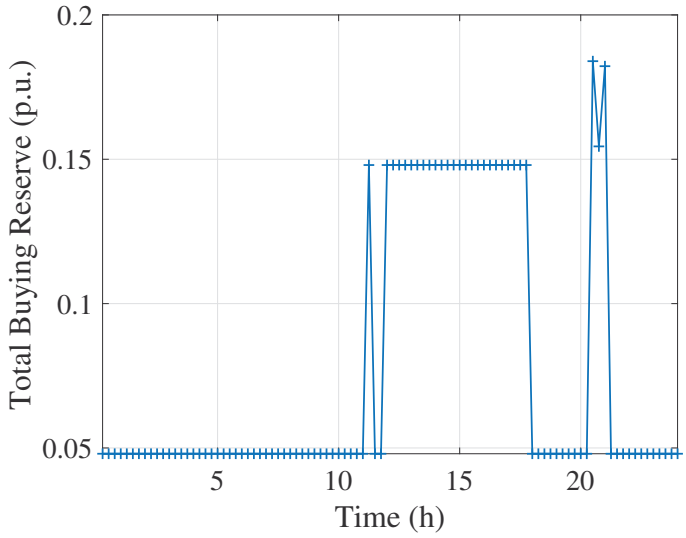

Figure 2.18: The reserve for buying power from the retail electricity market.

As shown in the Fig. 2.18 and Fig. 2.19, the reserve for buying/selling power from/to the retail electricity market is provided by three major components in the commercial campus: CHP units, ES units and EWHs. The total selling reserve is provided by the ramping-down reserve from CHP units, the ramping-down reserve from ES units, and the ramping-down reserve from EWHs, respectively. The total buying reserve is provided by, the ramping-up reserve from CHP units, and

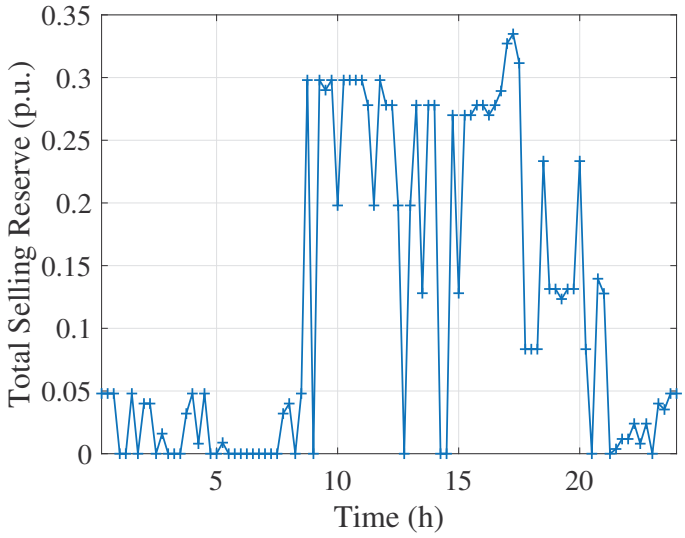

Figure 2.19: The reserve for selling power to the retail electricity market.

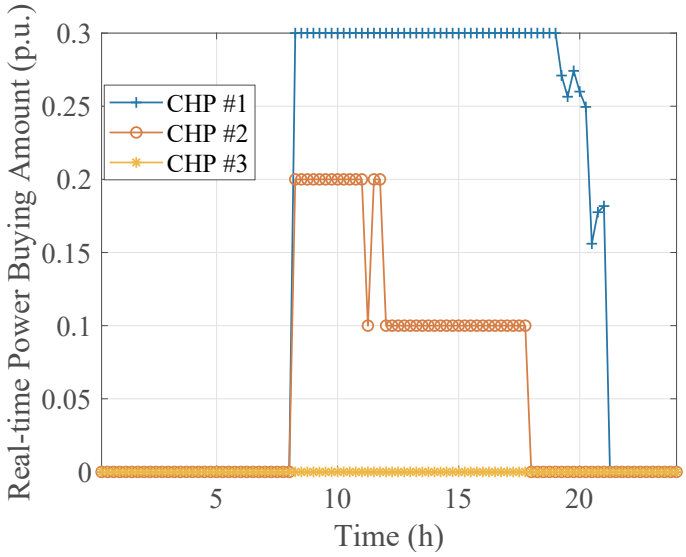

Figure 2.20: The power output of CHP units when the islanding issue occurs.

the ramping-up reserve from ES units, respectively. The islanding occurs at the 44-th time slot in the business hour, where the real-time power buying/selling from/to the retail electricity market is zero in that time slot as shown in Fig. 2.21 and Fig. 2.22. During the islanding period, the shorted power is supported by the CHP units and ES units, which increase the O&M costs only slightly but enhances the reliability of the commercial campus.

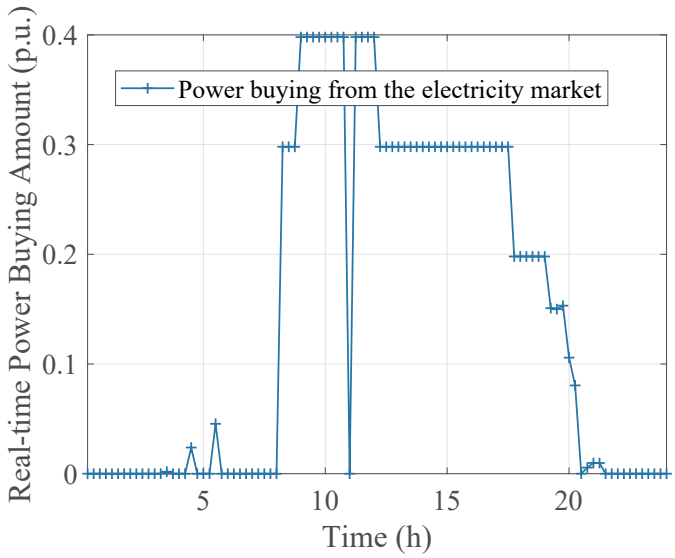

Figure 2.21: The power buying from the real-time retail electricity market.

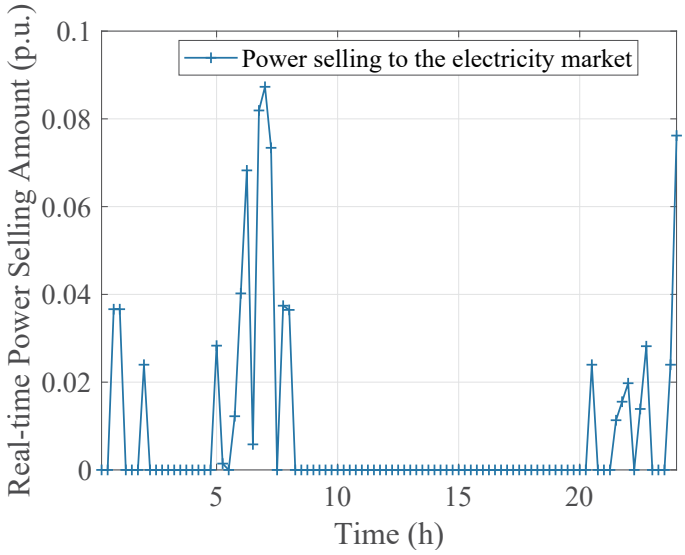

Figure 2.22: The power selling to the real-time retail electricity market.

2.5 Conclusions

In this section, we propose a novel safe reinforcement learning algorithm to provide resilient proactive scheduling decisions for the central controller of a CB. The correlation between different components with demand response capabilities is utilized to ensure the desired comprehensive comfort levels of the occupants can be maintained by the limited reserves. A deep-Q-network and a conditional-value-at-risk method are combined to mitigate the influence of extreme epochs on

the learning process. Extensive simulation results based on real-world data sets validate that the proposed SRL algorithm is capable of ensuring the resilience of a CB in an extreme weather event.

CHAPTER 3

Proactive Resilient Scheduling for Independent/Networked Microgrids with Extreme Events in the Distribution System

In addition to a commercial system, we further extend the proposed system to independent microgrids and networked microgrids in a distribution system. Moreover, we developed an innovative risk-constrained adaptive robust optimization approach to handle the uncertainties associated with the potential extreme weather event. The reason why we change the SRL algorithm to a RARO approach for the uncertainties of microgrids is that the total amount of actions the SRL algorithm can handle is limited, which is not suitable for the resilient proactive scheduling strategies of microgrids. Since the concepts of microgrids/networked microgrids under extreme weather event have been introduced in prior sections, therefore, we will mainly focus on the ssytem modeling in the networked microgrids and the way to implement the proposed proactive scheduling strategy as well as the simulation results based on the real-world data sets.

3.1 Introduction

Extreme events, such as earthquakes, tornadoes, hurricanes, floods and ice storms, are happening more and more often than ever before because of climate changes all over the world. Moreover, most of these extreme events are a danger to the resilience of power systems, especially distribution systems [40]. Distribution lines, substations, distributed energy resources (DERs), and consumers can be seriously damaged by strong winds and flooding, such as during Superstorm Sandy, Hurricane Harvey and Hurricane Irma. Unlike $N-1$ and $N-2$ contingency issues that have been extensively studied (mainly in the transmission system level), aforementioned extreme events could break down a whole distribution system which requires months to restore.

Resilience issues are receiving more attention due to the significant damage that extreme events inflict on power systems. A review of the resilience of power systems during natural disasters is

provided in [41], where the concepts of hardening, proactive scheduling, emergency response and restoration are perfectly defined, as shown in Fig. 3.1. The hardening and restoration aspects have been extensively studied [42, 43, 44, 45, 46, 47]; however, there are still several challenges that need to be tackled in the proactive scheduling and emergency response areas [48]. When facing an extreme event, in order to provide proactive operation and emergency response, rather than relying on passive methods, the continuous situational awareness issue needs to be considered. Additionally, ensuring the robustness of the distribution system prior to extreme events requires the system operator to handle a lot of uncertainties, such as: (i) weather uncertainty; (ii) reactions of various microgrid central controllers (MGCCs); (iii) resiliency issues related to critical buses and influential lines; and (iv) generation and load uncertainties. Thus, we mainly focus on proactive scheduling in this paper to address these challenges.

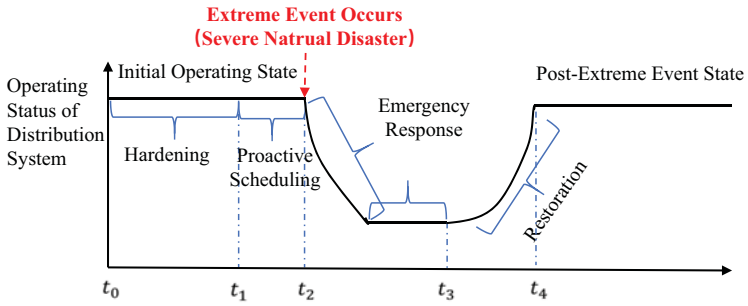

Figure 3.1: The four stages associated with the resilience of a distribution system.

Proactive resilient scheduling problem in the distribution system has attracted exponentially increasing attentions lately due to the aforementioned reasons. Specifically, networked microgrids have been adopted to enhance the resilience of distribution systems, where the proactive scheduling of MGCCs has become more important than ever before. A proactive operation strategy for enhancing resilience of microgrids using energy storage (ES) units is proposed in [49]. In addition, to optimally dispatch the mobile based ES units, a resilient routing and scheduling framework is implemented in [50]. Moreover, critical load resiliency is one of the major features in quantifying the resilience of a power system, especially during the extreme event. Thus, the transient stability, such as limits on frequency deviation and limits on bus voltage magnitude and phase angles are correlated together as constraints to provide resiliency control in [51]. Furthermore, not only the modeling of the resilience problem is important, but also how to handle the uncertainties as aforementioned becomes a priority issue that needs to be tackled.

Several optimization approaches have been adopted to handle uncertainties associated with extreme events. Some prior works [52, 53] consider a stochastic approach to handle such uncertainties, which requires hard-to-obtain probability distributions and adds a lot of computational burden to the problem-solving process. Since the computation time of proactive operation and

emergency response stages is limited, stochastic optimization is not suitable to handle resilient proactive scheduling problems. Additionally, a Markov chain approach is chosen by authors in [54] to make resilient proactive operation decisions when facing extreme events, where failure rates of different extreme events are introduced; however, when and where an extreme event will happen changes rapidly in each time slot. Thus, the adaptiveness of an approach is also very important. Other prior works consider conventional robust optimization to handle uncertainties [55], but do not consider risks of an extreme event developing beyond the proper "budget of uncertainty" that is suitable for the proactive scheduling stage, i.e., infeasible for the emergency response stage as shown in Fig. 3.1. Moreover, in order to handel such risks, a risk-limiting approach is introduced in [56], where joint probability density functions is provided for a MGCC to perform restoration. However, the robustness of the proactive scheduling cannot be guaranteed without cooperating with the robust optimization approach. Therefore, we introduce a risk-constrained adaptive robust optimization (RARO) approach to handle these uncertainties and the risks associate with them.

In this work, we mainly focus on developing a proactive approach to handle resilience issues of networked microgrids that are interconnected microgrids with multiple feeders, which is more difficult to handle compare to that of serial/parallel microgrids on a single feeder [57]. Moreover, one microgrid within the system of networked microgrids can benefit from other microgrids by facilitating high reliability for critical loads [58]. Specifically, MGCCs determine real and reactive power exchanges and select proper "budget of uncertainty" sets prior a potential extreme event. Then, after all uncertainties are revealed, MGCCs dispatch their DERs and exchange real and reactive power in real-time though only if tie-line and grid-connected buses are not influenced by an extreme event to make sure networked microgrids are stable and resilient.

We summarize our contributions in following aspects:

1. We present a comprehensive system model for networked microgrids' proactive resilient scheduling problems under extreme events.

2. We study not only the resilience of electricity in networked microgrids, but also their heating resiliency.

3. A RARO approach is proposed to handle the resilient proactive scheduling problem in networked microgrids. To the best of our knowledge, this approach has not been employed to handle uncertainties in resilient proactive operation problems previously.

4. Extensive simulation results show the effectiveness of our RARO approach that the system can survive from the beginning till the end of an extreme event.

3.2 System Modeling

3.2.1 Networked Microgrids

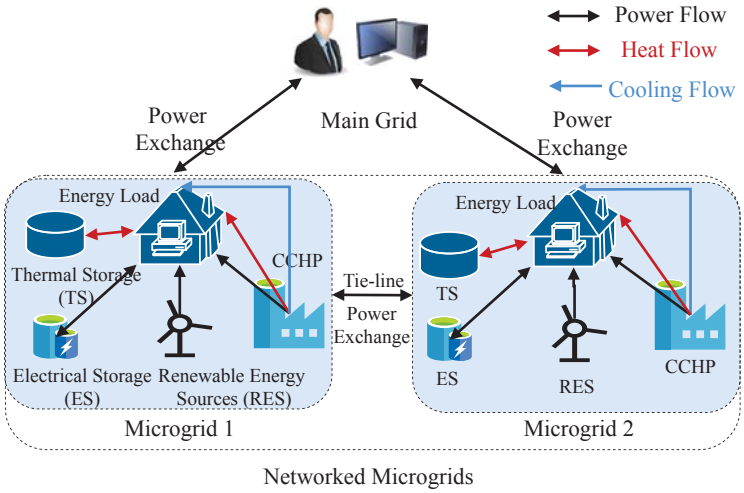

Figure 3.2: The networked microgrids with major components.

There are multiple interconnected microgrids with DERs, including distributed generation (DG) units and distributed storage (DS) units in a system of networked microgrids, as shown in Fig. 3.2. Networked microgrids are located downstream of a distribution substation and are managed by MGCCs. Additionally, the microgrids are connected to each other through tie-lines [59]. Specifically, a microgrid consists of trigeneration/combined cooling, heat and power (CCHP) units, renewable energy sources (RES), thermal storage (TS) units, electrical storage (ES) units, real and reactive power demand, cooling demand and heat demand. Each DER has a local controller (LC). MGCCs and LCs exchange information to achieve resilient and stable operation of networked microgrids.

3.2.1.1 Combined Cooling, Heat and Power

CCHP systems not only provide stable real and reactive power to fulfill the power demand but also supply either hot or chilled water to nearby buildings to support the heat and cooling demand through utilizing the waste heat from its power generation process [60]. When facing extreme events, the priority of a MGCC is to ensure the resilience of a microgrid. In order to provide sufficient power, heating and cooling for consumers, all CCHP units must be scheduled to stay on unless damaged and disconnected from a microgrid by an extreme event. Therefore, we have

following real and reactive power dynamic constraints:

$$\underline{P}_c \leq p_{c,t} \leq \overline{P}_c, \underline{Q}_c \leq q_{c,t} \leq \overline{Q}_c, \forall c, t \in [t_1, t_2) \tag{3.1}$$

$$\underline{P}_c O_{c,t_2} \leq p_{c,t} \leq \overline{P}_c O_{c,t_2}, \forall c, t \in [t_2, t_3] \tag{3.2}$$

$$\underline{Q}_c O_{c,t_2} \leq q_{c,t} \leq \overline{Q}_c O_{c,t_2}, \forall c, t \in [t_2, t_3], \tag{3.3}$$

where $\underline{P}_c$ and $\overline{P}_c$ are the lower bound and upper bound of the real power output $p_{c,t}$ of CCHP unit c. Parameters $\underline{Q}_c$ and $\overline{Q}_c$ are the lower bound and upper bound of the reactive power output $q_{c,t}$ of CCHP unit c. The t_1, t_2 and t_3 are time steps indicating the beginning of proactive scheduling stage, emergency response stage and restoration stage, respectively. O_{c,t_2} is a binary variable that indicating the grid-connection status of the CCHP unit c at time t_2 (when the extreme event occurs, also known as the emergency response stage). $O_{c,t_2} = 1$ represents that a CCHP unit c is still connected to the microgrid at the beginning of extreme event, where both active and reactive power can be generated by CCHP unit c after t_2. $O_{c,t_2} = 0$ denotes that a CCHP unit c is disconnected from the networked microgrids by an extreme event, where no power can be generated by CCHP unit c after t_2.

Additionally, when CCHP units are still on, the increment and decrement of the real power generation between two consecutive time slots need to follow ramping-up and ramping-down constraints:

$$\begin{aligned} &p_{c,t} - p_{c,t-1} \leq \mathrm{RU}_c, p_{c,t-1} - p_{c,t} \leq \mathrm{RD}_c, \forall c, t \in [t_1, t_2) \\ &p_{c,t} - p_{c,t-1} \leq \mathrm{RU}_c, \forall c, t \in [t_2, t_3] \\ &p_{c,t-1} - p_{c,t} \leq \mathrm{RD}_c(1 - O_{c,t_2}) + \overline{P}_c O_{c,t_2}, \forall c, t \in [t_2, t_3], \end{aligned} \tag{3.4}$$

where RU_c and RD_c denote the ramping up/down limits of the CCHP unit c.

3.2.1.2 Electrical and Thermal Storages

In our model, energy storage units, such as plug-in electric vehicles (PEVs) and hot water tanks, can provide elastic power and heat back-up when there is a forecasted extreme event. Based on the forecast of losing CCHP units or RES units, the ES and TS units can be relocated to the influenced buses, providing sufficient back-up of both power and heat for the critical load demand [61]. Thus, we have following storage dynamics and operating constraints for ES/TS units. First, we model the energy balance of ES units as follows:

$$E_{es,t} = E_{es,t-1} + p^+_{es,t}\eta^+_{es} - p^-_{es,t}/\eta^-_{es}, \forall es, t, \tag{3.5}$$

where $E_{es,t}$ denotes the power stored in an ES unit with initial power $E_{es,0}$. We use $p^+_{es,t}$ and $p^-_{es,t}$ as the rates of charging and discharging for ES unit es, and η^+_{es} and η^-_{es} as the efficiencies of charging and discharging for ES unit es, respectively.

Then, we have the physical limitations on the energy levels of ES units:

$$\underline{E}_{es} \leq E_{es,t} \leq \overline{E}_{es}, \forall es, t, \tag{3.6}$$

where the lower bound $\underline{E}_{es}$ and upper bound $\overline{E}_{es}$ are imposed to enhance the lifetime of the ES units.

Additionally, we have the physical limitations on the charging/discharging rate of ES units:

$$0 \leq p^+_{es,t} \leq P^+_{es}, 0 \leq p^-_{es,t} \leq P^-_{es}, \forall es, t, \tag{3.7}$$

where P^+_{es} and P^-_{es} are the upper bounds of the charging and discharging rates, respectively.

For TS units, we can model their storage dynamic and operating constraints similarly:

$$E_{ts,t} = E_{ts,t-1} + h^+_{ts,t}\eta^+_{ts} - h^-_{ts,t}/\eta^-_{ts}, \forall ts, t \tag{3.8}$$

$$0 \leq h^+_{ts,t} \leq H^+_{ts}, 0 \leq h^-_{ts,t} \leq H^-_{ts}, \underline{E}_{ts} \leq E_{ts,t} \leq \overline{E}_{ts}, \forall ts, t, \tag{3.9}$$

where $E_{ts,t}$ denotes the heating energy stored in the TS unit ts. Variables $h^+_{ts,t}$ and $h^-_{ts,t}$) are the charging and discharging rates of TS unit ts. Parameters η^+_{ts} and η^-_{ts}) represents the charging and discharging efficiency of TS unit ts. Also, H^+_{ts} and H^-_{ts} are the maximum charging and discharging rates of TS unit ts, respectively. $\underline{E}_{ts}$ and $\overline{E}_{ts}$ are the minimum and maximum energy levels of TS unit ts.

3.2.1.3 Critical and Non-Critical Energy Demand

In our model, in order to enhance the resilience of networked microgrids, we classify the real power demand as critical and non-critical power demand [62]. For critical power demand, the MGCC must ensure that adequate power generation is provisioned to meet their demand requirements within the operating horizon and cannot be curtailed. Parameter $D_{j,t}$ is introduced as the aggregated critical power demand of the bus j.

For non-critical power demand, they are allowed to be curtailed with a pre-defined reasonable penalty within a certain time interval (usually during the emergency response stage [t_2, t_3]). The specific amount of energy that can be curtailed is modeled as E_l, where each non-critical power demand l is allowed to be curtailed within the time interval $[T^b_l, T^e_l]$. Outside of this time interval, the non-critical power demand becomes "critical power demand", which must be satisfied without

interruption. For each non-critical load l, the load curtailment rate $p_{l,t}$ should be in the safe operation limitations of $[\underline{P}_l, \overline{P}_l]$ to prevent a potential cascading failure. The non-critical power demand requirement is expressed as:

$$\sum_{t=T_l^b}^{T_l^e} p_{l,t} \leq E_l, \underline{P}_l \leq p_{l,t} \leq \overline{P}_l, \forall l, t \in [T_l^b, T_l^e] \tag{3.10}$$

$$p_{l,t} = 0, \forall l, t \notin [T_l^b, T_l^e]. \tag{3.11}$$

Furthermore, as the heat demand is critical during extreme events such as snowstorms, we use H_t to represent the aggregated heat demand of all the buses in a system of networked microgrids.

3.2.1.4 Linearized AC Power Flow Equations

In our model, buses, lines and components in the networked microgrids suffer differently when facing extreme events [63]. For example, in one microgrid, the tie-line connected bus i and the point of common coupling (PCC) connected bus 0 is more influential. Besides, the tie-lines connecting various microgrids within the networked microgrids are also more influential than the distribution lines within each microgrid. Specifically, the components connected to the influential buses have higher risks of being damaged or disconnected from the networked microgrids. Thus, we mainly focusing on modeling the unique features related with these influential components. The conventional AC power flow equations are linearized through the following steps extended from [64]: (i) bus 0 and bus i are influential buses in each microgrid (denoted as I buses); (ii) $(V_{j,t} - V_{k,t})^2 \approx 0$, where $V_{j,t}$ is the voltage magnitude on bus j at time t; (iii) $\sin(\theta_{j,t} - \theta_{k,t}) \approx \theta_{j,t} - \theta_{k,t}$, and $\cos(\theta_{j,t} - \theta_{k,t}) \approx 1$, where $\theta_{j,t}$ denotes the voltage phase angle on bus j at time t; and (iv) the critical power demand are on the less-influential buses. Also, $\mathscr{N}_j^c$, $\mathscr{N}_j^l$, $\mathscr{N}_j^r$ and $\mathscr{N}_j^{es}$ are sets of CCHP, non-critical power demand, RES and ES units that are connected to bus j, respectively. Therefore, the real and reactive power injection equations are formulated as follows:

$$P_{I,t} = \sum_{c \in \mathscr{N}_I^c} p_{c,t} - p_t^{\mathrm{RT}} - \sum_{l \in \mathscr{N}_I^l} p_{l,t} + \sum_{r \in \mathscr{N}_I^r} w_{r,t} + \sum_{es \in \mathscr{N}_I^{es}} (p_{es,t}^- - p_{es,t}^+) + \sum_{l \in \mathscr{N}_I^l} p_{l,t}, \forall t \tag{3.12}$$

$$P_{j,t} = \sum_{c \in \mathscr{N}_j^c} p_{c,t} - D_{j,t}^p + \sum_{r \in \mathscr{N}_j^r} w_{r,t} + \sum_{es \in \mathscr{N}_j^{es}} (p_{es,t}^- - p_{es,t}^+), \forall j \neq I, t \tag{3.13}$$

where $P_{j,t}$ is the real power injection on bus j at time t. Variable p_t^{RT} indicates the actual real power exchange between networked microgrids and the main grid, as well as between each microgrid through tie-lines at time t. $w_{r,t}$ denotes the real power generation from the RES unit r at time t.

$$Q_{I,t} = \sum_{c \in \mathcal{N}_I^c} q_{c,t} - q_t^{\mathrm{RT}}, \forall t \tag{3.14}$$

$$Q_{j,t} = \sum_{c \in \mathcal{N}_j^c} q_{c,t} - D_{j,t}^q, \forall j \neq I, t. \tag{3.15}$$

where $Q_{j,t}$ is the reactive power injection on bus j at time t. Variable q_t^{RT} represents the real-time reactive power exchange between networked microgrids and the main grid, as well as between each microgrid through tie-lines at time t.

Similarly, the detailed linearized real and reactive power flow equations are formulated [65]:

$$P_{j,t} = (2V_{j,t} - 1)G_{j,j} + \sum_{k(k \neq j)} G_{j,k}(V_{j,t} + V_{k,t} - 1) + B_{j,k}(\theta_{j,t} - \theta_{k,t}), \forall (j,k), t \tag{3.16}$$

$$P_{j,k}^t = G_{j,k}(V_{j,t} - V_{k,t}) + B_{j,k}(\theta_{j,t} - \theta_{k,t}), \forall (j,k), t \tag{3.17}$$

where $G_{j,k}$ and $B_{j,k}$ are the real and imagine parts of the Y matrix of the networked microgrid. Variable $P_{j,k}^t$ denotes the real power flow from bus j to bus k at time t.

$$Q_{j,t} = -(2V_{j,t} - 1)B_{j,j} + \sum_{k(k \neq j)} -B_{j,k}(V_{j,t} + V_{k,t} - 1) + G_{j,k}(\theta_{j,t} - \theta_{k,t}), \forall (j,k), t \tag{3.18}$$

$$Q_{j,k}^t = B_{j,k}(V_{k,t} - V_{j,t}) + G_{j,k}(\theta_{j,t} - \theta_{k,t}), \forall (j,k), t. \tag{3.19}$$

Variable $Q_{j,k}^t$ represents the reactive power flow from bus j to bus k at time t.

3.2.1.5 Network Constraints

In order to ensure the stability and resilience of networked microgrids, we have the following lower and upper bounds on the voltage magnitude and phase angle [66]:

$$\underline{V}_j \leq V_{j,t} \leq \overline{V}_j, \underline{\theta}_j \leq \theta_{j,t} \leq \overline{\theta}_j, \forall j, t, \tag{3.20}$$

where $\underline{V}_j$ and $\overline{V}_j$ are the lower and upper bounds on the voltage magnitude at bus j. Parameters $\underline{\theta}_j$ and $\overline{\theta}_j$ are the lower and upper bounds on the voltage phase angle at bus j.

In addition, the resiliency of networked microgrids is also influenced by congestion, where the lower and upper bounds on real and reactive power flows on the distribution lines are listed as follows:

$$-\overline{P}_{j,k} \leq P_{j,k}^t \leq \overline{P}_{j,k}, -\overline{Q}_{j,k} \leq Q_{j,k}^t \leq \overline{Q}_{j,k}, \forall (j,k), t. \tag{3.21}$$

Parameters $\overline{P}_{j,k}$ and $\overline{Q}_{j,k}$ are the real and reactive power flow limitations on the distribution lines between bus j and bus k.

3.2.1.6 Energy Balance

As mentioned above, the heat loads are critical loads, (especially during extreme weather events, such as hurricane/strong wind/snow storm) that can be supplied the combination of CCHP units and TS units. Or when all the CCHP units are damaged or disconnected from the microgrid, the heat demand will be satisfied by the truck-based dispatchable TS unit only. Moreover, the heating (hot water in most cases) is not like the electricity, which can only be delivered within a short distance without decaying that significant [67]. Therefore, we assume that the heating cannot be transferred between microgrids, which can only be dispatched within a microgrid. Unlike heat demand H_t, the cooling demand C_t is assumed less critical, which is required to be satisfied before the extreme event. The heating and cooling balances are expressed as follows:

$$\sum_{c=1}^{N_c} \beta_c p_{c,t} \geq C_t, \sum_{c=1}^{N_c} \alpha_c p_{c,t} + \sum_{ts=1}^{N_{ts}} \left(h_{ts,t}^{-} - h_{ts,t}^{+}\right) \geq H_t, \forall t, \tag{3.22}$$

where we use power-to-heat ratio α_c and power-to-cooling ratio β_c to represent the relationship between power and useful heat and the cooling output of CCHP unit c.

3.2.2 Risk Management

In our model, uncertainties associated with an extreme event introduce a lot of risks into the networked microgrids. The risks reveal themselves in multiple aspects, as mentioned in previous sections. There are several ways to manage these risks, such as value-at-risk (VaR) and conditional-value-at-risk (CVaR) methods. In our model, we extend the CVaR method to handle risks associated with the resiliency issues in networked microgrids. The reason why we select this method is because we can obtain the proper "budget of uncertainty" [68] through managing risks of uncertainties. The trade-off between optimality and conservativeness is handled by the budget of uncertainty, where the decision of selecting the proper budget of uncertainty is made by MGCCs. Thus, the risk of selecting an improper budget of uncertainty must be ensured to be less than a certain confidence level ε. Therefore, we have the following risk management constraint:

$$0 \leq \varepsilon_x \leq \zeta_x, \forall x. \tag{3.23}$$

x denotes different kinds of uncertainties, Parameter ζ_x denotes the maximum allowed confidence level (usually 5%).

3.2.3 Total Cost

In each time slot t between proactive scheduling stage t_1 and emergency response stage t_3, the total cost of the networked microgrids is formulated as follows:

$$\begin{aligned}
&\sum_{c}^{N_c}(U_c^{\text{on}}O_{c,0}+U_c p_{c,t})+\sum_{l}^{N_l}U_l p_{l,t}\\
&+\sum_{es}^{N_{es}}U_{es}\left(p_{es,t}^{+}\eta_{es}^{+}+p_{es,t}^{-}/\eta_{es}^{-}\right)\\
&+\sum_{ts}^{N_{ts}}U_{ts}\left(h_{ts,t}^{+}\eta_{ts}^{+}+h_{ts,t}^{-}/\eta_{ts}^{-}\right)\\
&+[U_t^{\text{PE}}p_t^{\text{PE}}+U_t^{\text{RT}}(p_t^{\text{RT}}-p_t^{\text{PE}})+\delta_t]\\
&+\sum_{x}\kappa_x\varepsilon_x. \qquad (3.24)
\end{aligned}$$

Note that in equation (3.24), the operating cost of the CCHP units and the load curtailment cost are in the first line, while the second/third line represents the degradation and dispatch costs of the ES/TS units; the cost of power exchange is in the fourth line; and the last line denotes the cost associated with different risks. Parameter U_c^{on} is the minimum cost to maintain the operating status of CCHP unit c. Variable $O_{c,0}$ is the initial on/off status of the CCHP unit c. Parameter U_c denotes the generation cost of the CCHP unit c ($\$/kW$). Parameter U_l denotes the penalty from curtailed/influenced non-critical power demand. Parameters U_{es} and U_{ts} are the dispatch and degradation cost of the ES units and TS units, respectively. Variable p_t^{PE} represents the real power exchange schedule of each microgrid before the potential extreme event. Variable p_t^{RT} is the real power exchange of each microgrid in the real-time. Parameters U_t^{PE} and U_t^{RT} are pre-event and real-time power exchange prices, respectively. Variable δ_t denotes the power exchange mismatch cost, i.e., $\delta_t = \psi_t \left| p_t^{\text{RT}} - p_t^{\text{PE}} \right|$, where ψ_t is the penalty parameter. κ_x is a risk-averse parameter representing the relationship between the operating cost and the risk related with uncertainty x.

3.3 Problem Formulation

3.3.1 Uncertainty Set for RES Generation

As mentioned in previous sections, the robust optimization can handle various uncertainties through a pre-defined deterministic interval, such as $[\bar{w}_t - \hat{w}_t^{-}, \bar{w}_t + \hat{w}_t^{+}]$ for RES generation w. $\bar{w}_t$ represents the nominal value (i.e., forecasted value) of RES generation in time slot t. $\hat{w}_t^{-}$ and $\hat{w}_t^{+}$ are the maximum negative and positive deviations of RES generation in time slot t, respectively.

Coordinating with the budget of uncertainty Γ_w, we have the cardinality uncertainty set for RES generation as follows:

$$\mathscr{W} := \left\{ \mathbf{w} : w_t = \bar{w}_t + \hat{w}_t^+ v_t^+ - \hat{w}_t^- v_t^-, \forall t, v \in V \right\}, \tag{3.25}$$
$$V := \left\{ v : \sum_{t=t_1}^{t_3} \left(v_t^- + v_t^+ \right) \leq \Gamma_w, 0 \leq v_t^+, v_t^- \leq 1, \forall t \right\}.$$

v_t^+ and v_t^- are auxiliary variables indicating the degree of positive and negative deviation from the forecasted value $\bar{w}_t$.

3.3.2 Uncertainty Set for Critical Power Demand

When facing an extreme event, critical loads in networked microgrids may increase the total demand based on temperature change or other situations. Thus, it is important to consider potential demand changes when a disaster strikes since they cannot be curtailed. Similarly, we use $\bar{d}_t$ as the nominal value (i.e., forecasted value) of the critical load demand in period t. Then, the critical load demand d_t in time slot t can be expressed as $[\bar{d}_t - \hat{d}_t^-, \bar{d}_t + \hat{d}_t^+]$. $\hat{d}_t^-$ and $\hat{d}_t^+$ are the maximum negative and positive deviations of the critical load demand in period t, respectively. Similarly, coordinating with the budget of uncertainty Γ_d, we have the following cardinality uncertainty set for critical load demand:

$$\mathscr{D} := \left\{ \mathbf{d} : D_t = \bar{d}_t + \hat{d}_t^+ u^+ - \hat{d}_t^- u_t^-, \forall t, u \in U \right\}, \tag{3.26}$$
$$U := \left\{ u : \sum_{t=t_1}^{t_3} \left(u_t^- + u_t^+ \right) \leq \Gamma_d, 0 \leq u_t^+, u_t^- \leq 1, \forall t \right\}.$$

u_t^+ and u_t^- are auxiliary variables indicating the degree of positive and negative deviation from the forecasted value $\bar{d}_t$.

3.3.3 Uncertainty Set for Influential Buses

We use an auxiliary variable z_t to denote the resiliency issues of the influential buses and lines. When an extreme event happens, the real-time power exchange between networked microgrids and the main grid, as well as between each microgrid through tie-lines, may be different from the pre-event schedule due to damaged distribution lines and tie-lines. Also, we consider that all the tie-lines will be influenced at the same time, which is reasonable for a small distribution system. Similarly, coordinating with the budget of uncertainty Γ_I, we have the following cardinality

uncertainty set for influential buses and lines:

$$-\overline{P}_t z_t \leq p_t^{\mathrm{PE}} \leq \overline{P}_t z_t, -\overline{Q}_t z_t \leq q_t^{\mathrm{PE}} \leq \overline{Q}_t z_t, \forall t \tag{3.27}$$

$$-\overline{P}_t z_t \leq p_t^{\mathrm{RT}} \leq \overline{P}_t z_t, -\overline{Q}_t z_t \leq q_t^{\mathrm{RT}} \leq \overline{Q}_t z_t, \forall t, \tag{3.28}$$

where $\overline{P}_t$ and $\overline{Q}_t$ represent the line capacity of the real and reactive power, respectively.

$$\mathscr{Z} := \left\{ \mathbf{z} : \sum_{t=t_2}^{t_3} (1 - z_t) \leq \Gamma_I, 0 \leq z_t \leq 1, \forall t \right\}. \tag{3.29}$$

3.3.4 Uncertainty Set for CCHP Status

As mentioned in previous sections, O_{c,t_2} is used to denote resiliency issues of each CCHP unit c. When O_{c,t_2} is 0, the CCHP unit c is disconnected from the networked microgrids, which is influenced by an extreme event at t_2. When O_{c,t_2} is 1, the CCHP unit is connected to the networked microgrids, which is not influenced by the extreme event at t_2. Similarly, coordinating with the budget of uncertainty Γ_g, we have the following cardinality uncertainty set for CCHP status:

$$\mathscr{O} := \left\{ \mathbf{O} : \sum_{c=1}^{N_c} (1 - O_{c,t_2}) \leq \Gamma_g, O_{c,t_2} \in \{0,1\}, \forall c \right\}. \tag{3.30}$$

3.3.5 Two-Stage Adaptive Robust Risk-Constrained Optimization Formulation

We construct a two-stage adaptive robust risk-constrained optimization formulation to provide resilient proactive operation decisions for MGCCs. In the first stage, MGCCs make their own decisions regarding the pre-event power exchange schedule using both inter-exchange among microgrids and outer-exchange with the main grid, and select proper budgets of uncertainty to ensure the system can survive through the emergency response stage. Then the MGCCs dispatch each dispatchable unit in networked microgrids to ensure resilience by minimizing the operating cost with that all uncertainties have been revealed in the second stage. The adaptiveness of our approach is from the worst-case scenario that contains all the realizations of the uncertainties. Therefore, we

have the following two-stage RARO problem formulation:

$$\begin{aligned}
&\min_{z,O}\Bigg\{\sum_{c=1}^{N_{\mathrm{c}}} U_c^{on} O_{c,t_2} + \sum_{t=t_1}^{t_3} U_t^{\mathrm{PE}} p_t^{\mathrm{PE}} \\
&+\max_{w,d}\min_{p,h,x}\sum_{t=t_1}^{t_3}\Bigg[\sum_{c=1}^{N_{\mathrm{c}}} U_c p_{c,t} + U_t^{\mathrm{RT}}(p_t^{\mathrm{RT}} - p_t^{\mathrm{PE}}) + \delta_t \\
&\qquad + \sum_{es=1}^{N_{\mathrm{es}}} U_{es}\left(p_{es,t}^{+}\eta_{es}^{+} + p_{es,t}^{-}/\eta_{es}^{-}\right) \\
&\qquad + \sum_{ts=1}^{N_{\mathrm{ts}}} U_{ts}(h_{ts,t}^{+}\eta_{ts}^{+} + h_{ts,t}^{-}/\eta_{ts}^{-})\Bigg]\Bigg\} \\
&+\sum_{x}\kappa_x\varepsilon_x, \qquad (3.31)
\end{aligned}$$

subject to constraints (3.1)–(3.23).

3.4 Solution Methodology

For the simplicity of presenting the solution algorithm, we rewrite the original two-stage risk-constrained adaptive robust optimization formulation into a matrix form:

$$\begin{aligned}
&\min_{z,O}\left\{U^T(O,p) + \max_{w,d}\min_{p,h} U^T y(p,h,w,d)\right\} \\
&\quad + \kappa y(x) \\
&\text{s.t.}\quad AO \le p, Jz \le p, O, z \in \{0,1\} \qquad (3.32)\\
&\quad \Omega(p,h,w,d) = \Big\{Fy \le g, \qquad (3.33)\\
&\qquad\qquad Ty = w, \qquad (3.34)\\
&\qquad\qquad Ry = d\Big\}, \qquad (3.35)
\end{aligned}$$

where $\Omega(p,h,w,d)$ is the set of adaptive second-stage decisions based on first-stage decisions p and uncertainty sets z and O. y is the second-stage decisions, including p,h,w,d. Equation (3.32) represents the constraints related to only first-stage variables (3.1), (3.27), (3.29) and (3.30), where equation (3.33) collects constraints (3.4)–(3.11) and (3.14)–(3.22). Equation (3.34) accounts for constraints (3.12) and (3.25), which involve uncertain RES power generation. Equation (3.35) accounts for constraints (3.12) and (3.26), which include uncertain critical load demand.

3.4.1 Problem Reformulation

The formulation above is still a min-max-min problem, which cannot be solved directly by commercial solvers. Thus, as strong duality holds, we transform the inner min problem into its dual as a max problem:

$$\begin{aligned} \max_{w,d,\lambda,\mu,\varphi} \quad & -\lambda^T g + \mu^T w + \varphi^T d \\ \text{s.t.} \quad & -\lambda^T F + \mu^T T + \varphi^T R = U^T, \\ & \lambda \geq 0 \end{aligned} \tag{3.36}$$

where λ, μ and φ denote Lagrangian multipliers of constraints (3.33), (3.34) and (3.35), respectively. However, there are two bilinear terms, $\mu^T w$ and $\varphi^T d$, in (3.36), which makes the second-stage problem hard to solve. Thus, we need to linearize the bilinear terms through the Big-M method [69]. As shown in equations (3.25) and (3.36), RES generation is independent from all the other variables. Therefore, the realization of worst-case scenario w^* must be the extreme points of $\mathscr{W}$, where we assume $\hat{w}_t^+ = \hat{w}_t^-$.

Then, we can substitute (3.25) into the bilinear term $\mu^T w$ as follows:

$$\mu^T \vec{w} = \sum_{t=1}^{T} \left(\mu_t \bar{w}_t + \mu_t v_t^+ \hat{w}_t - \mu_t v_t^- \hat{w}_t \right). \tag{3.37}$$

Similarly, we can express $\varphi^T d$ as:

$$\varphi^T \vec{d} = \sum_{t=1}^{T} \left(\varphi_t \bar{d}_t + \varphi_t u_t^+ \hat{d}_t - \varphi_t u_t^- \hat{d}_t \right). \tag{3.38}$$

Then, we can transform the original bilinear dual problem into a linear one with the Big-M method [70]:

$$\begin{aligned} \max_{\varphi,\lambda,\sigma,\mu,\pi,v,u} \quad & -\lambda^T g + \sum_{t=t_1}^{t_3} (\mu_t \bar{w}_t + \sigma_t^+ \hat{w}_t - \sigma_t^- \hat{w}_t \\ & \qquad + \varphi_t \bar{d}_t + \pi_t^+ \hat{d}_t - \pi_t^- \hat{d}_t) \\ \text{s.t.} \quad & -\lambda^T F + \mu^T T + \varphi^T R = U^T, \lambda \geq 0 \\ & \sigma_t^+ \leq M u_t^+, \sigma_t^+ \leq \mu_t + M(1-u_t^+), \forall t \\ & \sigma_t^- \leq M u_t^-, \sigma_t^- \leq -\mu_t + M(1-u_t^-), \forall t \\ & \pi_t^+ \leq M v_t^+, \pi_t^+ \leq -\varphi_t^+ + M(1-v_t^+), \forall t \\ & \pi_t^- \leq M v_t^-, \pi_t^- \leq -\varphi_t^- + M(1-v_t^-), \forall t, \end{aligned} \tag{3.39}$$

where $\sigma_t^{\pm}$ and $\pi_t^{\pm}$ are auxiliary variables. M is a constant number that is large enough.

3.4.2 Column-and-Constraint Generation Algorithm

Combined with all the formulations from previous sections, we can finally reformulate the primal problem into the following mixed-integer linear programming (MILP) problem:

$$\begin{aligned}
\min \quad & U^T(O,p) + \theta + \kappa y_s(x_s) && \text{(3.40a)}\\
\text{s.t.} \quad & AO \le p, Jz \le p, O, z \in \{0,1\} && \text{(3.40b)}\\
& \theta \ge U^T y_s, s = 1,2,\ldots,S && \text{(3.40c)}\\
& Fy_s \le g, s = 1,2,\ldots,S && \text{(3.40d)}\\
& Ty_s = w_s, s = 1,2,\ldots,S && \text{(3.40e)}\\
& Ry_s = d_s, s = 1,2,\ldots,S. && \text{(3.40f)}
\end{aligned}$$

As mentioned in previous sections, the worst-case scenario of each set of uncertainty is independent from all others and can only occur at a set's upper and lower bound, which are finite. Thus, $\{\{w_s, O_s, z_s, d_s\}, s = 1,2,\ldots,S\}$ are the upper and lower bounds of the joint set $\mathscr{W} \times \mathscr{O} \times \mathscr{Z} \times \mathscr{D}$. To solve the problem in a reasonable solution time, we employ the column-and-constraint generation (C&CG) algorithm [71]. The basic idea of the C&CG algorithm is that a problem formulation with a partial enumeration of possible worst-case scenarios provides a valid relaxation to the original problem (3.40); we can calculate a lower bound by solving this relaxed problem (master problem). Hence, by adding a non-trivial possible worst-case scenario at each iteration, we can obtain a stronger lower bound. Meanwhile, at each iteration, we can find a corresponding upper bound by solving the second-stage problem (sub problem) with the first stage decisions being fixed. The algorithm terminates when the difference between the UB and the LB is within a small tolerance value.

Thus, we have the detailed C&CG algorithm as follows:

1. Set p_0 as the feasible first-stage decision with budget of uncertainty Γ_I and Γ_g. Then, solve the sub problem (3.39) with the initial conditions. After that, use the answer of w_1 and d_1 as the worst-case scenario. Let UB $= +\infty$ be the upper bound, LB $= -\infty$ be the lower bound, and 1 be the iteration number.

2. Solve the master problem (3.40) with the worst-case scenario. Determine the updated optimal first-stage decision and budget of uncertainty. Let LB $= U^T(O,p) + \theta + \kappa y_s(x_s)$.

3. Solve the sub problem (3.39) with the updated optimal solutions from Step 2. Make UB $=$ $\min\{\text{UB}, U^T(O,p) + \kappa y_s(x_s) + \rho^*\}$, where ρ^* is the updated value of the objective function.

4. If UB $-$ LB $\leq \varepsilon$, then stop. Otherwise, update s to $s+1$ and return to Step 2.

3.5 Simulation Results

We first evaluate our two-stage RARO approach in three steps: (i) we obtain the first-stage decisions p_t^{PE} and q_t^{PE} and choose proper budgets of uncertainty, while testing the convergence rate of the proposed solution algorithm; (ii) we solve the second-stage problem repeatedly for each first-stage decision with 1,000 randomly generated scenarios to show the adaptiveness of our proposed approach when facing extreme events; and (iii) we compare the capabilities of our approach with those of both the conventional robust approach and a deterministic approach to handling uncertainties. Then, we test the networked microgrids resilience under extreme conditions, especially when the extreme event develops to the emergency response stage between t_2 and t_3.

The proposed solution algorithm for the two-stage RARO model is implemented in Python 2.7. The reformulated MILP is solved with GUROBI 8.0.0 on a desktop with an Intel Core i7-7700 4.2 GHz CPU and 16GB of memory. We set 10^{-2} as the convergence tolerance.

3.5.1 Networked Microgrids

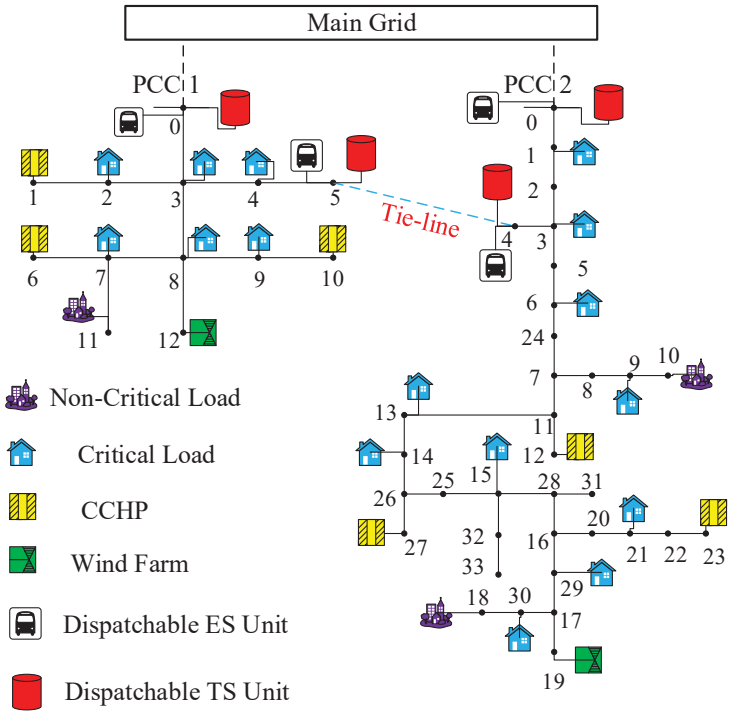

Figure 3.3: Two microgrids in a system of networked microgrids.

We consider two different microgrids in the set of networked microgrids, which are operated by the same MGCC. The networked microgrids are tested in a system with a modified IEEE 13-bus test feeder and a modified IEEE 34-bus test feeder [72], as shown in Fig. 3.3, where transformers, switches and voltage regulators are removed and the system is assumed to be balanced. The parameters of CCHP units are from [73]. The historical wind power generation data is from [74]. PEVs and hot water tanks are dispatched to the influential buses as forecasted that may be affected by the extreme event, where those parameters are as from [75]. The parameters of critical power loads are from [76], where non-critical power loads are 10% of the critical power loads. The begin and end time of the non-critical load curtailment time interval are t_1 and t_2, respectively. The load shedding cost is set to $1000\$/kWh$. The parameters of heat and cooling demand are from [77]. The pre-event and real-time power exchange prices are from [78], with proper scaling coefficients. The total time between t_1 and t_3 is set to six hours, where the proactive scheduling stage t_1 to t_2 takes four hours and the emergency response stage takes two hours, respectively. Each hour has four time slots t.

3.5.2 Results and Discussion

3.5.2.1 C&CG Algorithm Convergence

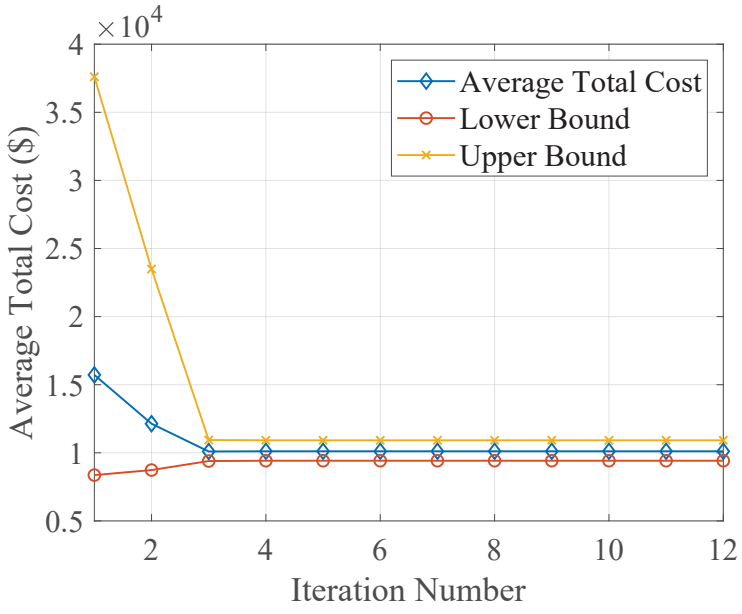

Figure 3.4: The average total cost and the lower/upper bound of networked microgrids with binormally distributed CCHP status.

We test the convergence property of the C&CG decomposition methodology for different

budgets of uncertainty: $\Gamma_w, \Gamma_d, \Gamma_I, \Gamma_g$ and obtain the optimal first-stage decisions. For the simplicity of demonstration, we show the simulation result of Γ_g for the convergence performance.

The UB and LB of the proposed approach with different budgets of uncertainty allotted for the CCHP status are shown in Fig. 3.4, where the convergence rate is three iterations. The iteration numbers for other uncertainty sets are from three to six. Therefore, the proposed C&CG algorithm can guarantee its convergence.

3.5.2.2 Budget of Uncertainty and System Resiliency

We test the proposed approach's ability to handle various uncertainties given an extreme event, based on several sets of randomly generated scenarios. The aim of this case study is to check the resiliency of the networked microgrids. The performance of the proposed approach is evaluated in two aspects: the average total cost and its standard deviation. The average total cost refers to the resiliency of the first-stage decisions and the guessing of the budget of uncertainties; its standard deviation indicates the adaptiveness of the proposed approach based on the first-stage decisions and the sets of budgets of uncertainty.

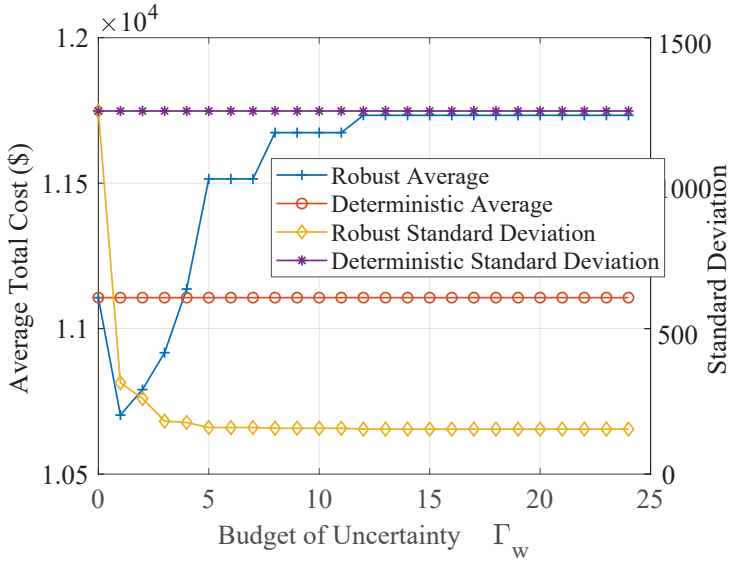

Figure 3.5: The average total cost and its standard deviation of networked microgrids with normal distributed wind power generation.

Firstly, we show the simulation results of the networked microgrids system that is influenced by the normally distributed wind power generation. One set of 1,000 normally distributed scenarios is generated, where the feasible region is from zero to $w_{\max}$ with mean $\bar{w}_t$ and standard deviation $\bar{w}_t/3$. Fig. 3.5 shows the average total cost for the networked microgrids for each Γ_w. We observe that when Γ_w is 1, the average total cost is the lowest, which is because the proposed approach

dispatches resources in the second stage, based on the wind power generation uncertainty set. As the wind power operating cost is zero, with more available wind power generation, the networked microgrids can reduce costs resulting from enabling expensive emergency options. In addition, we also compare the standard deviation of the total cost for each Γ_w, as shown in Fig. 3.5, which reduces rapidly when Γ_w is small and becomes steady with the increase of Γ_w. The reason is that a penalty occurs whenever there is a violation in the energy balance. The MGCC has to curtail the non-critical load to maintain system resiliency when the actual wind power generation is outside of the uncertainty set. Therefore, after considering all these aspects, the proper budget of uncertainty of wind power generation Γ_w is set to 2 in our test case.

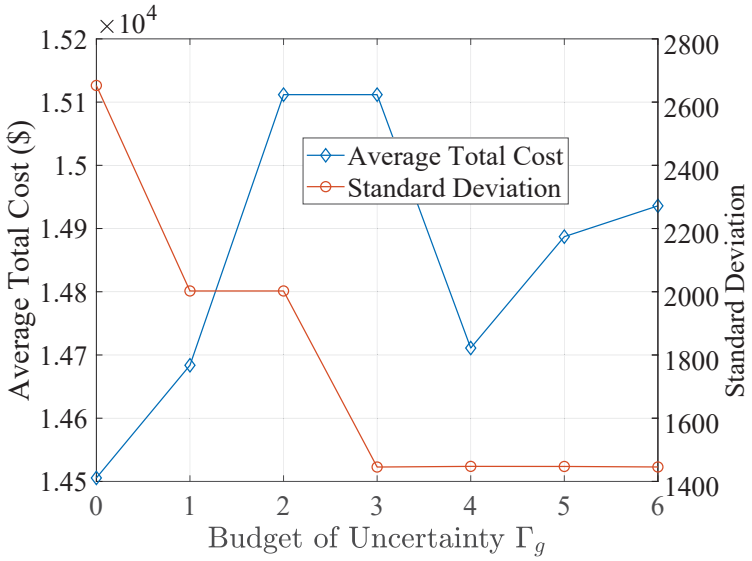

Figure 3.6: The average total cost and its standard deviation of networked microgrids with Bernoulli distributed CCHP units status.

Secondly, we focus on the CCHP status when an extreme event occurs, where other budget of uncertainty sets are remaining the same as the first settings. One set of 1,000 Bernoulli distribution scenarios is generated, where success probability p is set as 0.9. Fig. 3.6 shows the average total cost and standard deviation for the networked microgrids for each Γ_g. Based on the robustness evaluation criterions mentioned above, we set Γ_g to 4 for the proper budget of uncertainty of the CCHP connection status.

Thirdly, we focus on the tie-line connection status when an extreme event occurs, where other budget of uncertainty sets are remaining the same as the first settings. One set of 1,000 Bernoulli distribution scenarios is generated, where success probability p is set as 0.95. Fig. 3.6 shows the average total cost and standard deviation for the networked microgrids for each Γ_I. Similarly, based on the robustness evaluation criteria mentioned above, we set Γ_I to 3 for the proper budget

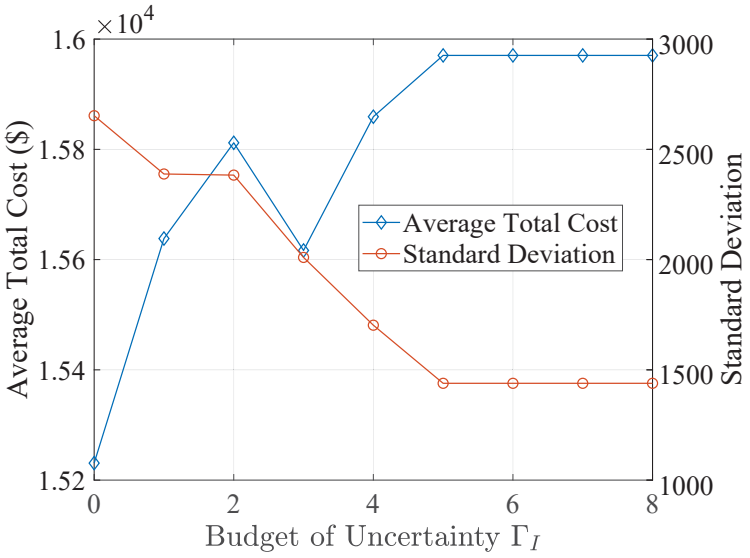

Figure 3.7: The average total cost and its standard deviation of networked microgrids with Bernoulli distributed influential buses status.

of uncertainty of the tie-line connection status. In the randomly generated 1,000 scenarios, the statuses of the tie-line are various in the 8 time slots between t_2 and t_3. In the worst-case scenarios, the tie-line between the two inter-connected microgrids are damaged, as well as the tie-lines connecting to the main grid through PCC 1 and PCC 2 from the beginning of the t_2. However, in most of the scenarios, the tie-lines will not be influenced from the beginning of the extreme event, (varies between $[t_2, t_3]$) which reflects in the Fig. 3.6. As shown in Fig. 3.6, based on both the average value and its standard deviation, we can see that Γ_I set to be 3 is the best choice to balance the cost and survivability of the networked microgrids. This is because the influence of the extreme event usually accelerates with the time, after 2-3 time slots (30-45 mins), the accelerated damage would break down the tie-lines as handled by the budget of uncertainty.

3.5.2.3 The Proposed RARO Approach versus Prior Approaches

We compare our RARO approach with prior approaches to show the capability of the proposed approach in handling uncertainties. In this comparison, we only consider the impact of uncertain wind power generation in networked microgrids.

We first compare the proposed approach with a deterministic approach with the uncertainty set defined above. $\Gamma_w = 0$ is the case for the deterministic approach, considering zero uncertainty and risk. For the proposed approach, we suggest $\Gamma_w = 2$, considering both the uncertainty and the risk. As shown in Fig. 3.5, both the average total cost and the standard deviation of the total cost of the proposed approach are lower than that of the deterministic approach. This is reasonable since the

proposed approach benefits from the first-stage decisions, making it adaptive to the realization of uncertain wind power generation.

Secondly, we compare the proposed approach with a conventional robust approach using the same settings. For the conventional robust approach, $\Gamma_w = 1$ is the optimal choice. However, compared with the proper budget of uncertainty $\Gamma_w = 2$ of our approach, the total load curtailment amount of the conventional robust approach, 194.23 kW, is much higher than that of our approach, 0 kW. The reason is that an extreme event can develop in the emergency response stage between t_2 to t_3, where a plan of $\Gamma_w = 1$ is not resilient enough to handle the situation.

Therefore, with the help of risk management, the proposed RARO approach can ensure the survivability of the networked microgrids system.

3.5.2.4 Networked Microgrids versus Independent Microgrids

Furthermore, the performance of a networked microgrids system and two independent microgrids under an extreme weather event is evaluated. In this case, we assume that the tie-line within the networked microgrids survived during the extreme weather event and the tie-lines connected to the main grid are down.

Compared with the performance tested for the uncertainty related with the on/off status of CCHP units in Fig. 3.6 and the uncertainty related with the random output from RES units in Fig. 3.5 for networked microgrids, the performance of two independent microgrids under the two aforementioned uncertainties is shown in Fig. 3.8 and Fig. 3.9.

Only the performance during the extreme event is shown for the two independent microgrids with normal distributed wind power generation in Fig. 3.9. This is because we mainly focus on the resiliency issues. As presented in the comparison, for both the average operating costs and the standard deviations of the two uncertainties, the networked microgrids are lower than that of the independent microgrids. This is reasonable since the real and reactive power that are exchanged through the tie-line can be utilized by the central controller of the networked microgrids to enhance the resilience of the system, where the two independent microgrids have to rely on their own components, especially when one CCHP unit is damaged in each microgrid by the extreme event.

As shown in Figs. 3.10, 3.11, 3.12 and 3.13, the two CCHP units are down from the beginning of the extreme event at time t_2, which influence the voltage magnitude of all the buses in both the 13-bus microgrid and the 34-bus microgrid. However, for the networked microgrids, the real and reactive power exchange through the tie-lie as shown in Fig. 3.14 help the central controller maintain the voltage magnitude within the predefined safety range of [0.9–1.1] (in per unit value). Moreover, the voltage magnitude of each bus is also maintained within the safety range for the independent microgrids, the reason is that based on the proposed RARO approach, where ES and TS units are dispatched to the influential buses to provide the back-up power and heating supply, the

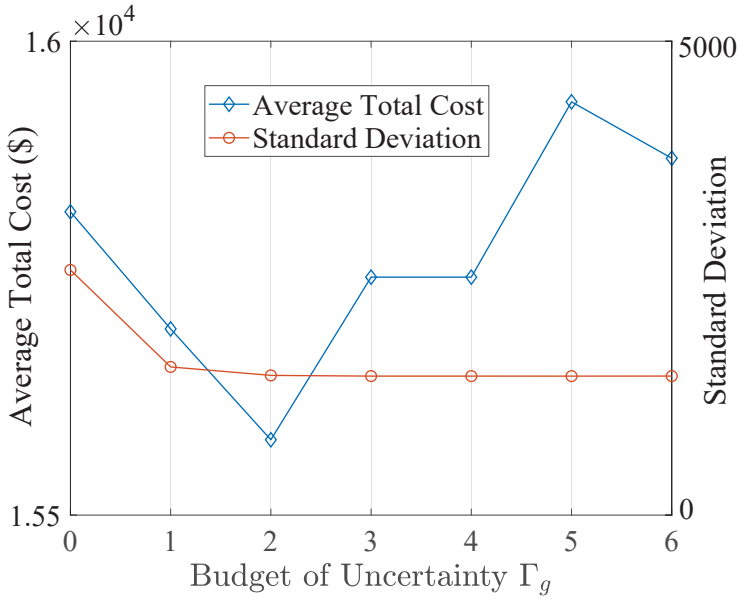

Figure 3.8: The average total cost and its standard deviation of two independent microgrids with Bernoulli distributed CCHP units status.

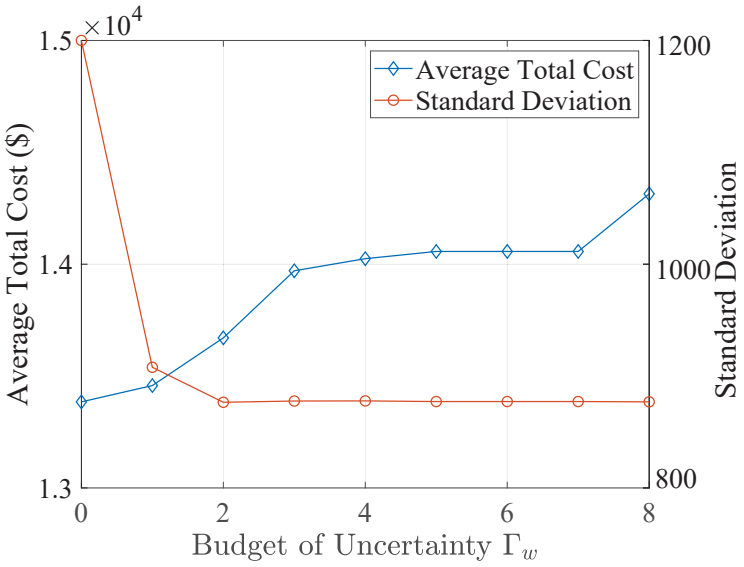

Figure 3.9: The average total cost and its standard deviation of two independent microgrids with normal distributed wind power generation.

resilience of the independent microgrids can still be ensured. Even though the voltage magnitude of the two systems are all within the safety range, the voltage magnitude of the 13-bus microgrid varies a lot as shown in Fig. 3.12, which is worse than that of the 13-bus microgrid in the networked microgrids. It is because the tie-line can not only transfer real-power, but also exchange reactive

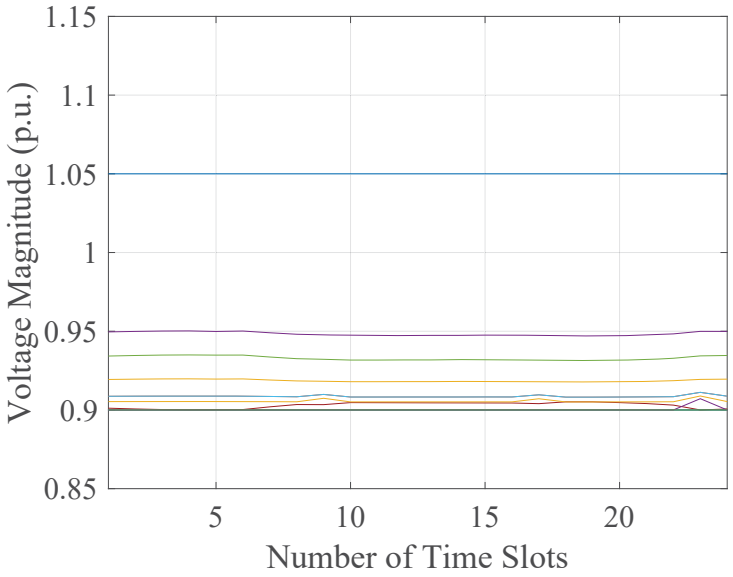

Figure 3.10: The voltage magnitude of each bus when two of the CCHP units are damaged for the 13-bus microgrid in networked microgrids.

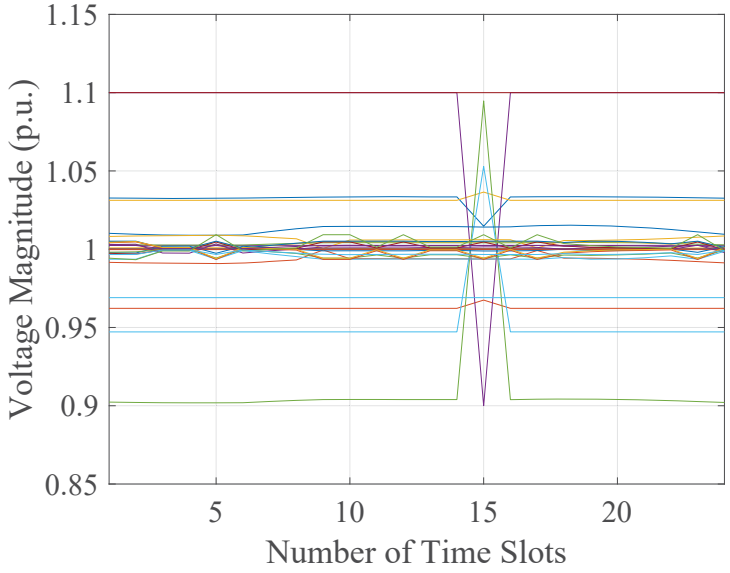

Figure 3.11: The voltage magnitude of each bus when two of the CCHP units are damaged for the 34-bus microgrid in networked microgrids.

power between the two microgrids, which contributes a lot in maintaining the voltage magnitude on each bus in the networked microgrids.

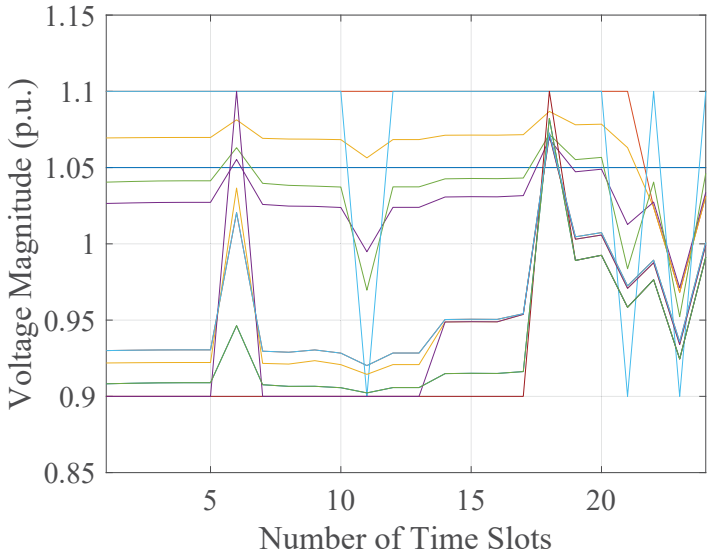

Figure 3.12: The voltage magnitude of each bus when two of the CCHP units are damaged for the independent 13-bus microgrid.

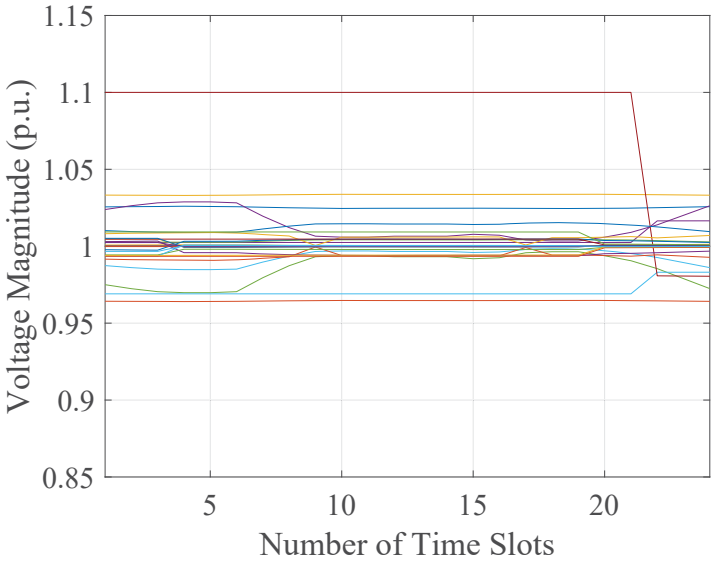

Figure 3.13: The voltage magnitude of each bus when two of the CCHP units are damaged for the independent 34-bus microgrid.

3.5.2.5 Sensitivity Analysis

In this part, we check the effectiveness and resilience of our system model by changing the parameters to simulate an extreme event; in particular, we change the load curtailment time interval in two scenarios. In scenario one, the ES and TS units are in networked microgrids that are pre-

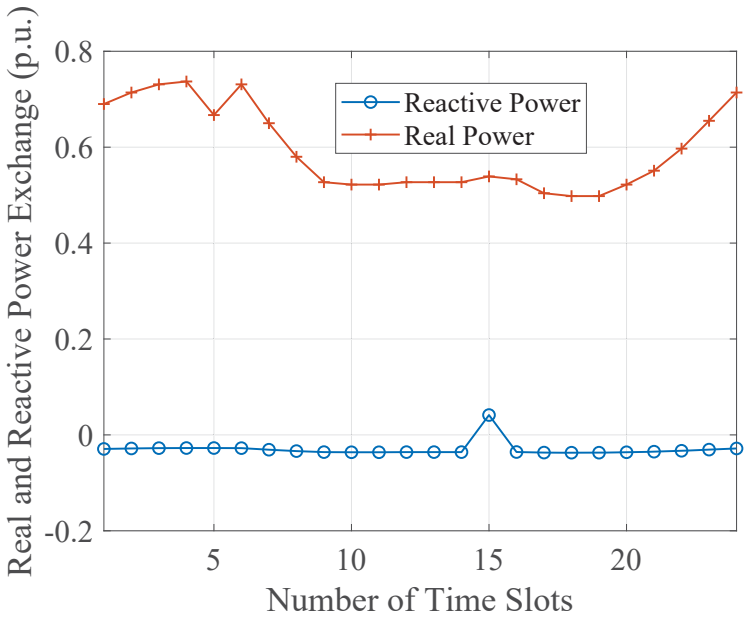

Figure 3.14: The real and reactive power exchange through the tie-line from the 13-bus microgrid to the 34-bus microgrid.

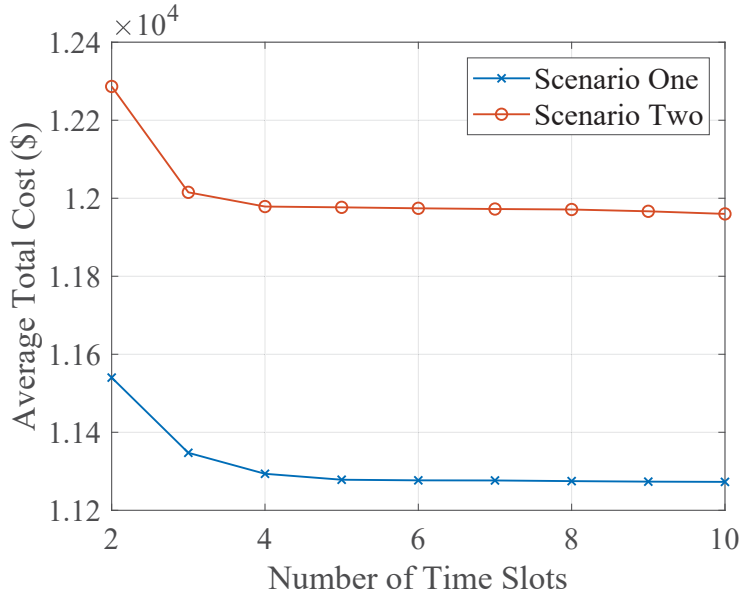

Figure 3.15: The average total cost of networked microgrids with different load curtailment time intervals.

scheduled to provide power and heat at the forecasted influenced buses. In scenario two, the ES and TS units are not in the networked microgrids. The impacts of the ES and TS units on the networked microgrids' resiliency are shown in Fig. 3.15. The average total cost of scenario one

is lower, where ES and TS units are coordinated by MGCCs to maintain the resiliency of the networked microgrids, while the only and expensive choice of scenario two is to perform load shedding. Additionally, with the increase of the load curtailment time interval, the networked microgrids' average total cost decreases. This is because with a longer allowed load curtailment time interval, a non-critical load can provide more flexibility when the TS and ES units are not on the influenced bus.

3.6 Conclusions

In this work, we proposed a risk-constrained adaptive robust optimization approach to provide proactive resilient scheduling decisions for networked microgrids central controllers under potential extreme events. Our objective is to ensure that after proactive resilient scheduling, most of the critical energy demand in the areas at risk of being influenced by the extreme event can still be satisfied by distributed generation units. A risk-constrained adaptive robust optimization approach has been developed to handle the risks and uncertainties associate with an extreme event. Extensive simulation results show that the approach we proposed can ensure the resilience of networked microgrids throughout an extreme event.

CHAPTER 4

Resilient Restoration for Distribution System Operators when Facing Extreme Events

A comprehensive framework to provide resilient restoration decisions for the distribution system operator (DSO) under extreme events is proposed in this work. Our objective is to maximize the system resilience by minimizing time slots required for load restoration. A bat algorithm is used to handle nonlinear and discrete characteristics of the proposed framework. Extensive simulation results show that the approach we proposed can ensure the resilience of the distributed system.

4.1 Introduction

Extreme events, such as earthquake, tornado, hurricane, flood and ice storm, are happening more and more often than ever before because of the climate change all over the world and most of them are dangerous to the power systems resilience, especially for the distribution systems. During Superstorm Sandy and Hurricane Harvey, distribution lines and substations are seriously damaged by wind and flooding. Moreover, with the development of modern society, the expectation of high quality electricity service put increasing pressure on distribution system operator (DSO) to enhance the resilience of the distribution grid against extreme events.

There are four time steps associate with the resilience of the distribution system: hardening, proactive scheduling, emergency response and restoration. The hardening part has already been extensively studied. However, there are still several challenges need to be faced in the system restoration part. When facing the extreme event, in order to provide the restoration rather through passive ways, the continuous situational awareness issue of the distribution system needs to be considered [79]. Moreover, the structure of the distribution system after the extreme event is seriously damaged, where the system reconfiguration is necessary to preform the restoration for the critical loads and buses. Furthermore, compared with earthquake and snowstorm, hurricane is

one of the major extreme events that has most of influence on the distribution system in the U.S.. Thus, we mainly focus on the resilient post-hurricane restoration part in this paper to face these challenges.

Resilience issues are receiving more attention due to the huge damage that extreme events bring to the power systems. A review on resilience of power system under natural disasters is provided in [41], where the time slot of hardening, emergency response and restoration are perfectly defined. In [80], a resilient distribution network planning problem is proposed to minimize the system damage, while coordinating the hardening and distributed generation resources allocation. Moreover, a stochastic programming approach for increasing resiliency of a distribution system exposed to an approaching wildfire is proposed in [81]. The uncertainties associate with the solar radiation, wind speed and wind direction that affect the progression of the wildfire and the production of stochastic distributed generators are considered. Furthermore, the resource allocation problem in distribution systems ahead of a coming hurricane is focused in [53]. Generation resources such as diesel oil and batteries are considered for allocation, which can be used to serve outage critical load in the post-hurricane restoration. Additionally, a proactive operation strategy to enhance system resilience during an unfolding extreme event is proposed in [54]. However, none of the papers mentioned above have considered all the distinct factors of restoration in distribution system.

In this work, we consider the resilience issues for distribution systems with multiple microgrids. Microgrids are adopted to enhance the resilience of distribution systems, where the restoration scheduling of microgrid central controllers (MGCCs) becomes important than before. The microgrids are different from conventional buck power systems in three aspects: (i) vastly deployed distributed energy resources (DERs) [82]; (ii) the DERs' sizes are very small (kW level) compared with conventional generation units (MW level) [83]; and (iii) the microgrids can be operated in both grid-connected mode and islanded mode, where the conventional power system cannot [84].

Specifically, the distribution system resilience problem operates in two stages. First, the MGCC determines the day-ahead bidding amount and the unit commitment decisions without knowing generation of RES units, extreme events conditions and potential reactions of MGCCs. Then, after the generation of RES units and extreme event conditions are revealed for each time slot, the microgrid dispatches its energy storage units, manages its controllable loads, and exchanges power with the main grid in real-time to meet the demand [85]. Therefore, we introduce the multi-time slots approach to handle these unique features.

In summary, the main contributions of this work are listed as follows:

- We propose a novel two-stage non-linear optimization formulation to model the post-hurricane resilience problem in distribution systems with microgrids.
- Bat algorithm is adopted to handle the nonlinear and discrete characteristics of the proposed

formulation.

- Extensive simulation results show that the proposed framework is effective and the proposed model is resilient.

4.2 Problem Formulation

This section explains the problem formulation of our proposed resilient post-hurricane restoration framework including the objective function and relevant constraints. For the simplicity of explanation about our framework, we assume there is one microgrid in the distribution system.

4.2.1 Microgrid Components

In our model, the microgrid has distributed generation (DG) units such as solar panels and wind turbines, distributed storage (DS) units such as plug-in electric vehicles (PEVs), controllable loads (CLs) such as heating, ventilating, and air-conditioning (HVAC) and uncontrollable loads such as lighting. The DG units in the microgrid are highly influenced by weather conditions and thus, are uncertain [86]. This problem can be overcome by coordinating DS units with DG units. When real-time DG is different from the forecasted amount, DS units can be used to mitigate imbalances caused by the weather uncertainty by charging or discharging [87]. CLs are both interruptible and adjustable, while the uncontrollable loads need to be satisfied at all times [88].

Microgrids are connected to the main grid through the points of common coupling (PCC). Each operating day in our model includes 24 time slots, with 1 hour per time slot.

4.2.2 Objective Function

In the post-hurricane analysis, the objective function is to maximize the system resilience by minimizing time slots required for load restoration. To this end, the system resilience curve after a typical extreme event is depicted in Fig. 4.1.

In Fig. 3.2, $F(t)$ shows the system performance function for different time intervals including: (i) hurricane event progress state $[t_e, t_{pe}]$; (ii) post-event degraded state $[t_{pe}, t_r]$; (iii) restoration state $[t_r, tpr]$; (iv) post-restoration state $[t_{pr}, t_{ir}]$; and (v)infrastructure recovery $[t_{ir}, t_{pir}]$, respectively. The main time interval which is available for maximizing the area bellow the system resilience curve is $[t_r, t_{ir}]$. Any time before t_r is engaged with hurricane and is not suitable for any special resilient strategy. At t_{ir}, the utility will start the normal recovery process and thus is out of the scope of this study.

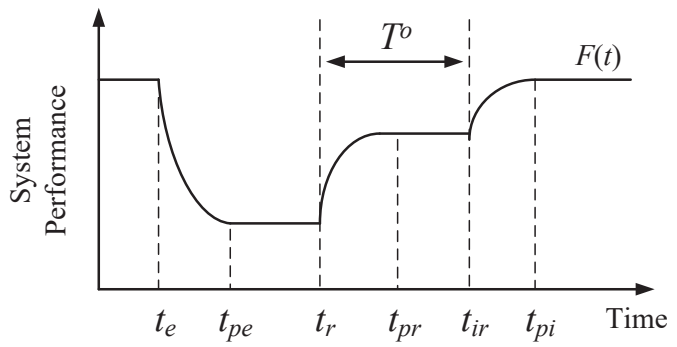

Figure 4.1: Network resilience curve after the hurricane.

According to Fig. 3.2, the system resilience objective function in the post-hurricane period is calculated as follows:

$$R = \gamma \int_{t_r}^{t_r+T^0} F(t)dt - G. \tag{4.1}$$

Here G represents the generators costs and γ is constant value to convert the $F(t)$ area into the equivalent dollar value R. In an electric grid, $F(t)$ is calculated as the total load value multiplied by its weighting factor as follows:

$$F(t) = \sum_l W_{l,t} P^D_{l,t}, t \in [t_r, t_r + T^0], \forall l \in Q, \tag{4.2}$$

where Q represents the set of branches l connected to the bus, W_l denotes the weighting factor of the bus l, $P^D_{l,t}$ is the total load demand on bus l, respectively.

Considering T^{sw} as the switching time through the reconfiguration, the R equation can be rewritten as below:

$$R = \gamma \int_{t_r}^{t_r+T^{sw}} (\sum_l W_{l,t} P^D_{l,t})dt - G = \gamma \sum_l W_l P^D_l T^{sw}_l - G, \forall l \in Q \tag{4.3}$$

where t is represented in T^{sw}_l after the reformulation.

Additionally, the total power generation cost from the DERs in the microgrid can be calculated as follows:

$$G = \sum_t (\sum_i \rho_i P_{i,t})\delta t, \forall i \in N_c, \forall t, \tag{4.4}$$

where $P_{i,t}$ represents the power generated from the i-th DG unit, ρ_i denotes the generation cost of the i-th DG unit as $\$/kW$.

4.2.3 Constraints

The resilient objective function R is maximized by meeting some equality and inequality constraints as follows:

4.2.3.1 AC Power Flow Equations

$$\overline{PL}_{m,n,t} = g_{m,n}V_{m,t}^2 - V_{m,t}V_{n,t}(g_{m,n}\cos(\theta_{m,t}-\theta_{n,t}) + b_{m,n}\sin(\theta_{m,t}-\theta_{n,t})), \forall m, \forall n, \forall t, \tag{4.5}$$

where $\overline{PL}_{m,n,t}$ is the real line flow from bus m to bus n in time t. $g_{m,n}$ and $b_{m,n}$ denote the conductance and susceptance of the line between bus m and bus n, respectively. $V_{m,t}$ and $V_{n,t}$ represent the voltage magnitude of bus m and bus n, respectively. $\theta_{m,t}$ and $\theta_{n,t}$ are the voltage phase angle of bus m and bus n, respectively.

Similarly, $\overline{QL}_{m,n,t}$ is the reactive line flow from bus m to bus n in time t.

$$\overline{QL}_{m,n,t} = -b_{m,n}V_{m,t}^2 - V_{m,t}V_{n,t}(-b_{m,n}\cos(\theta_{m,t}-\theta_{n,t}) + g_{m,n}\sin(\theta_{m,t}-\theta_{n,t})), \forall m, \forall n, \forall t. \tag{4.6}$$

Moreover, the most important part of the system restoration is the system reconfiguration.

$$-\Gamma(1-w_{m,n,t}) \leq PL_{m,n,t} - \overline{PL}_{m,n,t} \leq \Gamma(1-w_{m,n,t}), \forall m, \forall n, \forall t, \tag{4.7}$$

where Γ is an anxilary variable denotes the limitation of the reconfigured real line flow power associate with the remotely controlled switches. $w_{m,n,t}$ denotes the status of the remotely controlled switch on the line between bus m and bus n, which indicates the possibility of reconfiguration.

Additionally, when it is 0, the switch on the line is closed, i.e., there are power flowing through the line; when it is 1, the switch on the line is opened, i.e., there are no power flowing through the line. $PL_{m,n,t}$ represents the reconfigured line real power flow from bus m to bus n in time t.

$$-PL_{m,n}^{\max} w_{m,n,t} \leq PL_{m,n,t} \leq PL_{m,n}^{\max} w_{m,n,t}, \forall m, \forall n, \forall t, \tag{4.8}$$

where $PL_{m,n}^{\max}$ represents the limitation on the reconfigured real line power flow, which can prevent the contingency issues along with the system restoration process.

Similarly, we have following constraints for the reconfigured reactive line power flow [89]:

$$-\Gamma(1-w_{m,n,t}) \leq QL_{m,n,t} - \overline{QL}_{m,n,t} \leq \Gamma(1-w_{m,n,t}), \forall m, \forall n, \forall t. \tag{4.9}$$

$QL_{m,n,t}$ represents the reconfigured line reactive power flow from bus m to bus n in time t.

$$-QL_{m,n}^{\max} w_{m,n,t} \leq QL_{m,n,t} \leq QL_{m,n}^{\max} w_{m,n,t}, \forall m, \forall n, \forall t, \tag{4.10}$$

where $QL_{m,n}^{\max}$ represents the limitation on the reconfigured reactive line power flow, which can prevent the contingency issues along with the system restoration process.

4.2.3.2 Network Constraints

As the microgrid is connected to the main grid through the PCC, therefore, the security of the tie-line is very important for the MGCC in order to maintain the resilience of the microgrid with sufficient power supply. Hence, we need to take the network limitations into consideration. First, the real power delivery between the main grid and the microgrid must stay within the physical limitation of the tie-line:

$$-P_M^{\max} \leq P_{M,t} \leq P_M^{\max}, \forall t, \tag{4.11}$$

where $\pm P_M^{\max}$ denotes the upper bound and lower bound of the tie-line, respectively. $P_{M,t}$ represents the power delivery between the main grid and the microgrid.

Additionally, the stability of the microgrid is equally important as its resiliency. Thus, limitations of the voltage magnitude and phase angle of each bus in the microgrid need to be satisfied:

$$V_l^{\min} \leq V_{l,t} \leq V_l^{\max}, -\theta_l^{\max} \leq \theta_{l,t}\theta_l^{\max}, \forall l, \forall t, \tag{4.12}$$

where $V_l^{\min}$ and $V_l^{\max}$ represents the lower bound and upper bound of the voltage magnitude on bus l, $\pm\theta_l^{\max}$ denotes the upper bound and lower bound of the voltage phase angle of bus l, respectively.

4.2.3.3 Constraints of DG Units

In the microgrid, most of the DG units are combined heat and power (CHP) units that can generate useful heat and power simultaneously, which can significantly improve the overall efficiency of the microgrid [90]. Even though the DG units in the microgrid are usually smaller compared with the conventional generation units, such as coal-fired power plants, they still need to follow certain physical rules. We assume that the DG units do not need to absorb reactive power to start up and the DG units have been turned off for a sufficient time period before the operating day. For instance, the DG unit can only generate power when it is started up, which is impossible for it to generate power when it is shut down:

$$P_i^{\min} I_{i,t} \leq P_{i,t} \leq P_i^{\max} I_{i,t}, \forall i, \forall t, \tag{4.13}$$

where $P_{i,t}$ denotes the real power generated from DG unit i in time t. $P_i^{\min}$ and $P_i^{\max}$ are the lower bound and upper bound of the physical limitation for i-th DG unit in the microgrid, respectively. $I_{i,t}$ is a binary variable indicates the on/off status of the DG unit i, when it is 1, the DG unit i is on;

when it is 0, the DG unit i is off.

Additionally, the limitations on the DG unit ramping up and ramping down rate are shown as follows:

$$P_{i,t} - P_{i,t-1} \leq UR_i, \forall i, \forall t, \tag{4.14}$$

$$P_{i,t-1} - P_{i,t} \leq DR_i, \forall i, \forall t, \tag{4.15}$$

where UR_i and DR_i denote the maximum ramping up and ramping down rate of DG unit i between two periods.

Moreover, in order to guarantee the lifetime of DG units, they can not be turned on/off before warming/cooling for a certain period, which is also known as the uptime and downtime constraints [91]:

$$T_{i,t}^{on} \geq UT_i(I_{i,t} - I_{i,t-1}), \forall i, \forall t, \tag{4.16}$$

$$T_{i,t}^{off} \geq DT_i(I_{i,t-1} - I_{i,t}), \forall i, \forall t, \tag{4.17}$$

where $T_{i,t}^{on}$ and $T_{i,t}^{off}$ denote the time that the DG unit i must stay on and off, respectively. UT_i and DT_i are the minimum uptime and downtime of DG unit i.

4.2.3.4 Constraints of DS Units

As mentioned before, when adopting RES units in the microgrid, DS units are also implemented in the microgrid to help the CHP units to mitigate the energy imbalance caused by the uncertainties brought by the RES units. The DS units are commonly considered as PEVs in the microgrid, which can provide both vehicle to grid (V2G) and grid to vehicle (G2V) [92]. Furthermore, the DS units can also considered as back-up generators when performing system restoration after the hurricane. Thus, it is important to consider the physical limitations on the DS units. Firstly, the charging and discharging process of DS units must be operating within the safety range:

$$P_{e,t} \leq P_{e,t}^{dch,\max} u_{e,t} - P_{e,t}^{ch,\min} v_{e,t}, \forall e, \forall t, \tag{4.18}$$

$$P_{e,t} \geq P_{e,t}^{dch,\min} u_{e,t} - P_{e,t}^{ch,\max} v_{e,t}, \forall p, \forall t, \tag{4.19}$$

where $P_{e,t}$ denotes the charing and discharging rate of the DS unit e, that is bounded by the maximum and minimum charging and discharging rate $P_{e,t}^{ch,\max}$, $P_{e,t}^{ch,\min}$, $P_{e,t}^{dch,\max}$ and $P_{e,t}^{dch,\min}$, respectively. Additionally, $u_{e,t}$ and $v_{e,t}$ are binary variables that indicate the discharging and charging status of the DS unit e, when $u_{e,t}$ is 1, the DS unit e is discharging and when $v_{e,t}$ is 1, the DS unit e is charging.

However, the DS unit can not be charged and discharged at the same time [93]. Therefore, we

have following status constraint for the DS units:

$$u_{e,t} + v_{e,t} \leq 1, \forall e, \forall t. \tag{4.20}$$

This can be used to determine the DS unit e is either charging or discharging.

Moreover, in order to enhance the lifetime of the DS units, the state-of-charge (SOC) and charging and discharging time must be considered.

$$C_{e,t} = C_{e,t-1} - P_{e,t}, C_e^{\min} \leq C_{e,t} \leq C_e^{\max}, \forall e, \forall t, \tag{4.21}$$

where $C_{e,t}$ denotes the remaining energy inside the DS unit e, which is related to the previous status and the charging/discharging rate. Additionally, it is bounded by the physical limitation of the DS units as upper bound $C_e^{\max}$ and lower bound $C_e^{\min}$, which is usually 10% to 90% of the DS unit's total capacity.

Furthermore, the charging time $T_{e,t}^{ch}$ and discharging time $T_{e,t}^{ch}$ are guaranteed by the minimum charging time MC_e and minimum discharging time MD_e. When the status of charing and discharging changes, the time limitations begin to count.

$$T_{e,t}^{ch} \geq MC_e(u_{e,t} - u_{e,t-1}), T_{e,t}^{dch} \geq MD_e(v_{e,t} - v_{e,t-1}), \forall e, \forall t. \tag{4.22}$$

4.3 Optimization Algorithm

Due to the nonlinear and discrete characteristics of the proposed formulation, this paper makes use of bat algorithm (BA) to solve the problem. BA is a meta-heuristic optimization algorithm which mimics the echolocation process to find the optimal solution. To this end, four main rules are used to lead the random solutions in the bat population [94]: (i) each bat X_j with the velocity of V_j generates an especial pulse with the frequency and loudness of f_j and A_j, respectively; (ii) loudness constant A_j diminishes from a large value to a low value; (iii) echolocation phenomenon helps the bats to distinguish food from a barrier; and (iv) as time passes, the frequency f_j and rate r_j are updated dynamically.

Initially a random bat population is generated. Each bat represents a solution for the proposed optimization problem. After calculating the objective function, the bat position is updated as below:

$$V_j^{new} = V_j^{old} + f_j(G_{best} - X_j), X_j^{new} = X_j^{old} + V_j^{new}, f_j = f_j^{\min} + \phi_1(f_j^{\max} - f_j^{min}), \forall j \in \Omega, \tag{4.23}$$

where ϕ_1 is a pre-defined weighting factor. G_{best} is an initial bat population number. Ω denotes the

set of solutions in BA.

In a second stage, BA uses a random movement to improve the population. Therefore, a random value (β) is generated and compared with r_j. If that is larger than r_j, a new solution around the bat X_j is generated:

$$X_j^{new} = X_j^{old} + \varepsilon A_{mean}^{old}, \forall j \in \Omega. \tag{4.24}$$

In the this formulation, ε is a random value in the range of $[-1,1]$ and A_{mean}^{old} equals the mean value of the bats loudness. In the case that β is smaller than r_j, another random solution X_j^{new} is generated. The new solution is accepted only if the following two conditions are satisfied:

$$\beta \leq A_j, f(X_j) \leq f(G_{best}), \forall j \in \Omega. \tag{4.25}$$

After each iteration, the loudness and rate parameter are updated as follows:

$$A_j^{new} = \alpha A_j^{old}, r_j^{Iter+1} = r_0[1 - \exp(-\gamma Iter)], \forall j \in \Omega, \tag{4.26}$$

where α and γ are constant values and $Iter$ is the iteration number.

Therefore, the problem we proposed can be solved iteratively [95].

4.4 Simulation Results

All simulations are implemented on a laptop with a 2.20 GHz Intel Core i7-2670 CPU and 8GB RAM.

4.4.1 Numerical Settings

This section uses IEEE 32-bus network as a microgrid test system. Fig. 3.3 shows the single line diagram of the network incorporating fuel cell (FC), micro turbine (MT) and Photovoltaics (PV). The hurricane path is shown by blue line in this picture. Microgrid is assumed to have 5 tie switches (normally open) which are shown by dotted lines and 32 sectionalizing switches (normally closed) which are shown by solid lines. A main circuit breaker is located at the main feeder to make it possible for microgrid to go islanded if necessary. There is a sectionalizer at the beginning of each feeder to make it possible for reconfiguration. The other numerical settings are the same as [96].

DG characteristics such as capacity, ramp up and down and generation costs are shown in Table 4.1.

Table 4.1: Parameters for DGs

Type	Min Power (kW)	Max Power (kW)	Bid ($/kWh)	Start-up/ Shut-down Cost ($)
PV	-	-	2.584	-
FC	80	1000	0.294	1.65
MT-1	100	1500	0.457	0.96
MT-2	100	1500	0.457	0.96

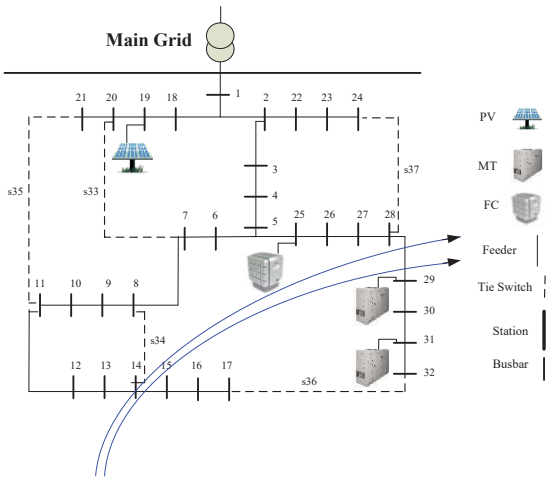

Figure 4.2: Schematic of the RMG with DGs and PEV fleet.

4.4.2 Simulation Results

We test our proposed model in three different scenarios to show the effectiveness of our approach.

4.4.2.1 Scenario 1

Ignore reconfiguration and DGs are OFF. In this scenario, there is no restoration and the microgrid receives normal utility crew help after $t_r + T^0$. As shown in Fig. 4.3, the total energy that is not supplied in scenario 1 is the highest among all the three scenarios. This is reasonable because there is no reconfiguration process considered in scenario1, while all DGs are OFF. The demand remains the same but the MGCC cannot provide enough generation without the help of DGs. Moreover, the utility crew is scheduled after $t_r + T^0$, which means that the generation units are backed up slower than the expected speed, where the demand are still the same as the scheduled amount. This could result in cascading failure in the microgrid as well as in the distribution system.

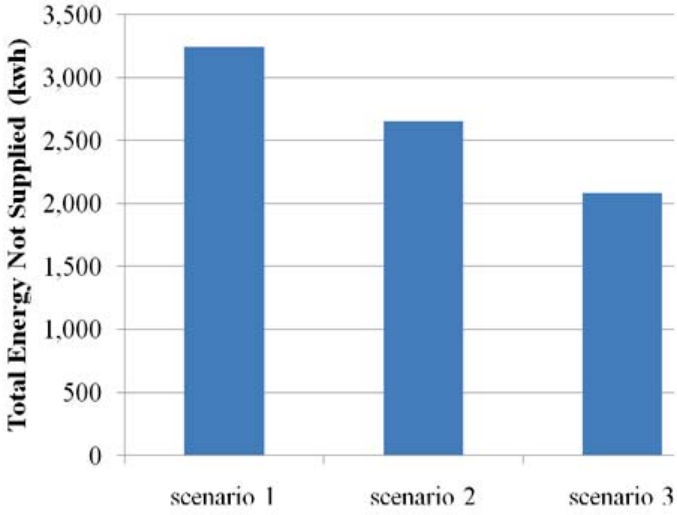

Figure 4.3: Comparative plot of total energy not supplied for three scenarios.

4.4.2.2 Scenario 2

Ignore reconfiguration but DGs are ON. In this scenario, some loads are restored by DGs at time t_r. As shown in the Fig. 4.3, the scenario 2 is better than the scenario 1 but worse than the scenario 3. This is because the reconfiguration process is not considered in scenario 2 but the DGs are ON and some loads are restored by DGs are time t_r. The DGs can provide part of the generation to some of the loads while the others are lost. Also, the loads are backed up as expected which reduces the unsupported loads by the end of the time slots.

4.4.2.3 Scenario 3

Consider reconfiguration and DGs are ON. In this scenario, restoration process is made by DGs as well as switching at time t_r. As presented in Fig. 4.3, the scenario 3 is the best among all the three scenarios. As mentioned above, the scenario 3 considers the reconfiguration process as well as the DGs are ON. Therefore, with the on time help of the utility crews, the MGCC can maintain the resilience of the microgrid after the extreme event.

4.4.2.4 Sensitivity Analysis

Table 4.2 shows the detailed simulation results for all scenarios. According to these results, the microgrid lost several buses in scenario 1, where the resilience-related performance is the worst among all the three scenarios. The scenario 3 is the best among all the three scenarios with smallest load losses and highest resilience-related performance. With the reconfiguration process and all

Table 4.2: Simulation Results for Different Scenarios

Case Number	Bus Without Power	Resilience Objective Function ($)
Scenario 1	13,14,15,16,17,29,30,31,32	42,667.14
Scenario 2	13,14, 15, 16, 17	44,529.20
Scenario 3	13,14	45,098.67

the DGs as well as the on time help from the utility crews, the microgrid can provide resilient restoration after the hurricane.

4.5 Conclusion

In this work, a comprehensive framework to provide resilient restoration decisions for the distribution system operator under extreme events has been proposed. The objective of maximizing the system resilience by minimizing time slots required for load restoration has been realized. Bat algorithm has been adopted to handle nonlinear and discrete characteristics of the proposed framework. Extensive simulation results show that the approach we proposed can ensure the resilience of the distributed system.

CHAPTER 5

Conclusions and Future Work

5.1 Conclusions

In this dissertation, several novel algorithms, such as safe reinforcement learning algorithm and risk-constrained adaptive robust optimization approach are proposed to provide resilient proactive scheduling strategies, emergency response strategy and restoration strategy for central controllers in the distribution system. Microgrids are proposed to serve as single entities from the perspective of the distribution system operator to enhance the resilience of the distribution system, reduce the distribution system operator's control burden and improve the power quality of the distribution system. Uncertainties related with the extreme weather events such as power generation of distributed generators, intermittent load demand, point-of-common-coupling/tie-line conditions, and trend/trace of the extreme weather event are tackled through a combination of optimization approaches, artificial intelligence algorithms and risk management methods. Extensive simulation results based on real-world data sets show that the proposed novel algorithms based proactive scheduling strategies, emergence response strategy and restoration strategy can ensure the resilience of the distribution system in a real-world environment.

5.2 Future Work

There are still challenges that remain in the emergency response stage, such as the issues of situation awareness, dispatching a rescue team, and relay protection. We will continue our study on the highly correlated uncertainties associate with the extreme events in the future research. We will develop a novel method with the vine copula approach to describe the dependence between various uncertainties and reduce the total dimension of the resilience related problems.

BIBLIOGRAPHY

[1] M. Fisher, J. Apt, and F. Sowell, "The economics of commercial demand response for spinning reserve," *Energy Systems*, vol. 9, no. 1, pp. 3–23, 2018.

[2] N. D. Laws, K. Anderson, N. A. DiOrio, X. Li, and J. McLaren, "Impacts of valuing resilience on cost-optimal pv and storage systems for commercial buildings," *Renewable energy*, vol. 127, pp. 896–909, 2018.

[3] E. Vrettos, F. Oldewurtel, and G. Andersson, "Robust energy-constrained frequency reserves from aggregations of commercial buildings," *IEEE Trans on Power Systems*, vol. 31, no. 6, pp. 4272–4285, 2016.

[4] S. Papadopoulos, C. E. Kontokosta, A. Vlachokostas, and E. Azar, "Rethinking hvac temperature setpoints in commercial buildings: The potential for zero-cost energy savings and comfort improvement in different climates," *Building and Environment*, vol. 155, pp. 350–359, 2019.

[5] Z. Liang, Q. Alsafasfeh, T. Jin, H. Pourbabak, and W. Su, "Risk-constrained optimal energy management for virtual power plants considering correlated demand response," *IEEE Trans on Smart Grid*, vol. 10, no. 2, pp. 1577–1587, 2017.

[6] C.-W. Ten and Y. Tang, *Electric Power Distribution Emergency Operation*. Taylor & Francis Group, 2018.

[7] A. M. Dizaji, M. Saniei, and K. Zare, "Resilient operation scheduling of microgrid using stochastic programming considering demand response and electric vehicles," *Journal of Operation and Automation in Power Engineering*, vol. 7, no. 2, pp. 157–167, 2019.

[8] H. Lei, S. Huang, Y. Liu, and T. Zhang, "Robust optimization for microgrid defense resource planning and allocation against multi-period attacks," *IEEE Trans on Smart Grid*, vol. 10, no. 5, pp. 5841–5850, 2019.

[9] Y. Zhou, M. Shahidehpour, Z. Wei, Z. Li, G. Sun, and S. Chen, "Distributionally robust co-optimization of energy and reserve for combined distribution networks of power and district heating," *IEEE Trans on Power Systems*, vol. 35, no. 3, pp. 2388–2398, 2019.

[10] M. Elsayed, M. Erol-Kantarci, B. Kantarci, L. Wu, and J. Li, "Low-latency communications for community resilience microgrids: A reinforcement learning approach," *IEEE Trans on Smart Grid*, vol. 11, no. 2, pp. 1091–1099, 2019.

[11] C. Robinson, B. Dilkina, J. Hubbs, W. Zhang, S. Guhathakurta, M. A. Brown, and R. M. Pendyala, "Machine learning approaches for estimating commercial building energy consumption," *Applied energy*, vol. 208, pp. 889–904, 2017.

[12] S. Yao, J. Gu, P. Wang, T. Zhao, H. Zhang, and X. Liu, "Resilient load restoration in microgrids considering mobile energy storage fleets: A deep reinforcement learning approach," *arXiv preprint arXiv:1911.02206*, 2019.

[13] M. Tavakoli, F. Shokridehaki, M. F. Akorede, M. Marzband, I. Vechiu, and E. Pouresmaeil, "Cvar-based energy management scheme for optimal resilience and operational cost in commercial building microgrids," *International Journal of Electrical Power & Energy Systems*, vol. 100, pp. 1–9, 2018.

[14] B. Lötjens, M. Everett, and J. P. How, "Safe reinforcement learning with model uncertainty estimates," in *2019 International Conference on Robotics and Automation (ICRA)*, pp. 8662–8668, IEEE, 2019.

[15] R. Phillips, L. Troup, D. Fannon, and M. J. Eckelman, "Do resilient and sustainable design strategies conflict in commercial buildings? a critical analysis of existing resilient building frameworks and their sustainability implications," *Energy and Buildings*, vol. 146, pp. 295–311, 2017.

[16] L. Klein, J.-y. Kwak, G. Kavulya, F. Jazizadeh, B. Becerik-Gerber, P. Varakantham, and M. Tambe, "Coordinating occupant behavior for building energy and comfort management using multi-agent systems," *Automation in construction*, vol. 22, pp. 525–536, 2012.

[17] H. Pourbabak, J. Luo, T. Chen, and W. Su, "A novel consensus-based distributed algorithm for economic dispatch based on local estimation of power mismatch," *IEEE Trans on Smart Grid*, vol. 9, no. 6, pp. 5930–5942, 2017.

[18] C. D. Korkas, S. Baldi, I. Michailidis, and E. B. Kosmatopoulos, "Occupancy-based demand response and thermal comfort optimization in microgrids with renewable energy sources and energy storage," *Applied Energy*, vol. 163, pp. 93–104, 2016.

[19] Q. Zhou, Z. Li, Q. Wu, and M. Shahidehpour, "Two-stage load shedding for secondary control in hierarchical operation of islanded microgrids," *IEEE Trans on Smart Grid*, vol. 10, no. 3, pp. 3103–3111, 2018.

[20] D. T. Nguyen and L. B. Le, "Joint optimization of electric vehicle and home energy scheduling considering user comfort preference," *IEEE Trans on Smart Grid*, vol. 5, no. 1, pp. 188–199, 2014.

[21] Z. Liang, D. Bian, X. Zhang, D. Shi, R. Diao, and Z. Wang, "Optimal energy management for commercial buildings considering comprehensive comfort levels in a retail electricity market," *Applied Energy*, vol. 236, pp. 916–926, 2019.

[22] F. Chang, T. Chen, W. Su, and Q. Alsafasfeh, "Charging control of an electric vehicle battery based on reinforcement learning," in *2019 10th International Renewable Energy Congress (IREC)*, pp. 1–63, March 2019.

[23] J. Duan, K. Zhang, and L. Cheng, "A novel method of fault location for single-phase microgrids," *IEEE Trans on Smart Grid*, vol. 7, no. 2, pp. 915–925, 2015.

[24] A. Khodaei, "Microgrid optimal scheduling with multi-period islanding constraints," *IEEE Trans on Power Systems*, vol. 29, no. 3, pp. 1383–1392, 2013.

[25] G. Liu, M. Starke, B. Xiao, Z. Zhang, and K. Tomsovic, "Microgrid optimal scheduling with chance-constrained islanding capability," *Electric Power Systems Research*, vol. 145, pp. 197–206, 2017.

[26] V. Bui, A. Hussain, H. Kim, and Y. Im, "Optimal energy management of building microgrid networks in islanded mode considering adjustable power and component outages," *Energies*, vol. 11, no. 9, p. 2351, 2018.

[27] S. Acharya, M. El-Moursi, A. Al-Hinai, A. Al-Sumaiti, and H. Zeineldin, "A control strategy for voltage unbalance mitigation in an islanded microgrid considering demand side management capability," *IEEE Trans on Smart Grid*, vol. 10, no. 3, pp. 2558–2568, 2018.

[28] Z. Li and Y. Xu, "Optimal coordinated energy dispatch of a multi-energy microgrid in grid-connected and islanded modes," *Applied Energy*, vol. 210, pp. 974–986, 2018.

[29] Y. Zong, D. Kullmann, A. Thavlov, O. Gehrke, and H. W. Bindner, "Application of model predictive control for active load management in a distributed power system with high wind penetration," *IEEE Trans on Smart Grid*, vol. 3, no. 2, pp. 1055–1062, 2012.

[30] H. Pourbabak and A. Kazemi, "Islanding detection method based on a new approach to voltage phase angle of constant power inverters," *IET Generation, Transmission & Distribution*, vol. 10, no. 5, pp. 1190–1198, 2016.

[31] A. Naug, I. Ahmed, and G. Biswas, "Online energy management in commercial buildings using deep reinforcement learning," in *2019 IEEE International Conference on Smart Computing (SMARTCOMP)*, pp. 249–257, IEEE, 2019.

[32] R. T. Rockafellar and S. Uryasev, "Optimization of conditional value-at-risk," *Journal of risk*, vol. 2, pp. 21–42, 2000.

[33] T. Chen, Q. Alsafasfeh, H. Pourbabak, and W. Su, "The next-generation us retail electricity market with customers and prosumersa bibliographical survey," *Energies*, vol. 11, no. 1, p. 8, 2018.

[34] S. Xiang, L. Chang, B. Cao, Y. He, and C. Zhang, "A novel domestic electric water heater control method," *IEEE Trans on Smart Grid*, 2019.

[35] C. Cui, Y. Zou, L. Wei, and Y. Wang, "Evaluating combination models of solar irradiance on inclined surfaces and forecasting photovoltaic power generation," *IET Smart Grid*, vol. 2, no. 1, pp. 123–130, 2019.

[36] S. Xu, H. Pourbabak, and W. Su, "Distributed cooperative control for economic operation of multiple plug-in electric vehicle parking decks," *International Trans on Electrical Energy Systems*, vol. 27, no. 9, p. e2348, 2017.

[37] H. Pourbabak, A. Ajao, T. Chen, and W. Su, "Fully distributed ac power flow (acpf) algorithm for distribution systems," *IET Smart Grid*, vol. 2, no. 2, pp. 155–162, 2019.

[38] Z. Liang, Q. Alsafasfeh, and W. Su, "Proactive resilient scheduling for networked microgrids with extreme events," *IEEE Access*, vol. 7, pp. 112639–112652, 2019.

[39] H. Pourbabak, Q. Alsafasfeh, and W. Su, "Fully distributed ac optimal power flow," *IEEE Access*, vol. 7, pp. 97594–97603, 2019.

[40] P. Hines, J. Apt, and S. Talukdar, "Trends in the history of large blackouts in the united states," in *Power and Energy Society General Meeting*, pp. 1–8, IEEE, 2008.

[41] Y. Wang, C. Chen, J. Wang, and R. Baldick, "Research on resilience of power systems under natural disastersa review," *IEEE Trans on Power Systems*, vol. 31, no. 2, pp. 1604–1613, 2016.

[42] M. Panteli, D. N. Trakas, P. Mancarella, and N. D. Hatziargyriou, "Power systems resilience assessment: Hardening and smart operational enhancement strategies," *Proceedings of the IEEE*, 2017.

[43] C. Chen, J. Wang, and D. Ton, "Modernizing distribution system restoration to achieve grid resiliency against extreme weather events: An integrated solution," *Proceedings of the IEEE*, vol. 105, no. 7, pp. 1267–1288, 2017.

[44] A. C. Reilly, G. L. Tonn, C. Zhai, and S. D. Guikema, "Hurricanes and power system reliabilitythe effects of individual decisions and system-level hardening," *Proceedings of the IEEE*, 2017.

[45] A. Arif and Z. Wang, "Networked microgrids for service restoration in resilient distribution systems," *IET GTD*, vol. 11, no. 14, pp. 3612–3619, 2017.

[46] B. Chen, C. Chen, J. Wang, and K. L. Butler-Purry, "Sequential service restoration for unbalanced distribution systems and microgrids," *IEEE Trans on Power Systems*, vol. 33, no. 2, pp. 1507–1520, 2017.

[47] Y. Wang, Y. Xu, J. He, C.-C. Liu, K. P. Schneider, M. Hong, and D. T. Ton, "Coordinating multiple sources for service restoration to enhance resilience of distribution systems," *IEEE Trans on Smart Grid*, 2019.

[48] M. H. Amirioun, F. Aminifar, and M. Shahidehpour, "Resilience-promoting proactive scheduling against hurricanes in multiple energy carrier microgrids," *IEEE Trans on Power Systems*, 2018.

[49] A. Hussain, V.-H. Bui, and H.-M. Kim, "A resilient and privacy-preserving energy management strategy for networked microgrids," *IEEE Trans on Smart Grid*, vol. 9, no. 3, pp. 2127–2139, 2018.

[50] S. Lei, C. Chen, H. Zhou, and Y. Hou, "Routing and scheduling of mobile power sources for distribution system resilience enhancement," *IEEE Trans on Smart Grid*, 2018.

[51] Y. Xu, C.-C. Liu, K. P. Schneider, F. K. Tuffner, and D. T. Ton, "Microgrids for service restoration to critical load in a resilient distribution system," *IEEE Trans on Smart Grid*, vol. 9, no. 1, pp. 426–437, 2018.

[52] D. N. Trakas and N. D. Hatziargyriou, "Optimal distribution system operation for enhancing resilience against wildfires," *IEEE Trans on Power Systems*, 2017.

[53] H. Gao, Y. Chen, S. Mei, S. Huang, and Y. Xu, "Resilience-oriented pre-hurricane resource allocation in distribution systems considering electric buses," *Proceedings of the IEEE*, vol. 105, no. 7, pp. 1214–1233, 2017.

[54] C. Wang, Y. Hou, F. Qiu, S. Lei, and K. Liu, "Resilience enhancement with sequentially proactive operation strategies," *IEEE Trans on Power Systems*, vol. 32, no. 4, pp. 2847–2857, 2017.

[55] A. Gholami, T. Shekari, and S. Grijalva, "Proactive management of microgrids for resiliency enhancement: An adaptive robust approach," *IEEE Trans on Sustainable Energy*, 2017.

[56] Z. Wang, C. Shen, Y. Xu, F. Liu, X. Wu, and C.-C. Liu, "Risk-limiting load restoration for resilience enhancement with intermittent energy resources," *IEEE Trans on Smart Grid*, vol. 10, no. 3, pp. 2507–2522, 2018.

[57] A. Barnes, H. Nagarajan, E. Yamangil, R. Bent, and S. Backhaus, "Tools for improving resilience of electric distribution systems with networked microgrids," *arXiv preprint arXiv:1705.08229*, 2017.

[58] K. P. Schneider, F. K. Tuffner, M. A. Elizondo, C.-C. Liu, Y. Xu, S. Backhaus, and D. Ton, "Enabling resiliency operations across multiple microgrids with grid friendly appliance controllers," *IEEE Trans on Smart Grid*, vol. 9, no. 5, pp. 4755–4764, 2018.

[59] Y. Tang, C. Ten, C. Wang, and G. Parker, "Extraction of energy information from analog meters using image processing," *IEEE Trans on Smart Grid*, vol. 6, no. 4, pp. 2032–2040, 2015.

[60] J. Hernández-Santoyo and A. Sánchez-Cifuentes, "Trigeneration: an alternative for energy savings," *Applied Energy*, vol. 76, no. 1, pp. 219–227, 2003.

[61] B. Zhang, W. Li, T. Chen, and W. Su, "A simulation platform for energy-efficient dynamic commuter transit using electric vehicles," in *2016 IEEE Transportation Electrification Conference and Expo, Asia-Pacific (ITEC Asia-Pacific)*, pp. 812–817, IEEE, 2016.

[62] Y. Tang, S. Zhao, C. Ten, and K. Zhang, "Enhancement of distribution load modeling using statistical hybrid regression," in *IEEE Power Energy Society Innovative Smart Grid Technologies Conference (ISGT)*, pp. 1–5, 2017.

[63] D. Wei, X. Deng, X. Zhang, Y. Deng, and S. Mahadevan, "Identifying influential nodes in weighted networks based on evidence theory," *Physica A: Statistical Mechanics and its Applications*, vol. 392, no. 10, pp. 2564–2575, 2013.

[64] M. E. Khodayar, M. Barati, and M. Shahidehpour, "Integration of high reliability distribution system in microgrid operation," *IEEE Trans on Smart Grid*, vol. 3, pp. 1997–2006, December 2012.

[65] Y. Tang, C. Ten, and L. E. Brown, "Switching reconfiguration of fraud detection within an electrical distribution network," in *Resilience Week (RWS)*, pp. 206–212, September 2017.

[66] Z. Bingxue, L. Tingting, T. Yachen, and L. Guangyi, "Research on power equipment life-cycle management technology based on graph database," *Electric Power Information and Communication Technology*, vol. 17, no. 3, pp. 1–7, 2019.

[67] Z. Liang and Y. Guo, "Optimal energy management for microgrids with cogeneration and renewable energy sources," in *Smart Grid Communications (SmartGridComm), 2015 IEEE International Conference on*, pp. 647–652, IEEE, 2015.

[68] D. Bertsimas and M. Sim, "The price of robustness," *Operations research*, vol. 52, no. 1, pp. 35–53, 2004.

[69] R. Jiang, J. Wang, and Y. Guan, "Robust unit commitment with wind power and pumped storage hydro," *IEEE Trans on Power Systems*, vol. 27, pp. 800–810, May 2012.

[70] T. Ding, R. Bo, W. Gu, and H. Sun, "Big-m based miqp method for economic dispatch with disjoint prohibited zones," *IEEE Trans on power systems*, vol. 29, no. 2, pp. 976–977, 2014.

[71] B. Zeng and L. Zhao, "Solving two-stage robust optimization problems using a column-and-constraint generation method," *Operations Research Letters*, vol. 41, no. 5, pp. 457–461, 2013.

[72] M. A. Mohamed, T. Chen, W. Su, and T. Jin, "Proactive resilience of power systems against natural disasters: A literature review," *IEEE Access*, vol. 7, pp. 163778–163795, 2019.

[73] Z. Liang and W. Su, "Game theory based bidding strategy for prosumers in a distribution system with a retail electricity market," *IET Smart Grid*, vol. 1, no. 3, pp. 104–111, 2018.

[74] T. Chen, A. Mutanen, P. Järventausta, and H. Koivisto, "Change detection of electric customer behavior based on amr measurements," in *2015 IEEE Eindhoven PowerTech*, pp. 1–6, IEEE, 2015.

[75] B. Zhang, H. Lim, S. Xu, and W. Su, "Distance-oriented hierarchical control and ecological driving strategy for hevs," *IET Electrical Systems in Transportation*, vol. 9, no. 1, pp. 44–52, 2018.

[76] Y. Tang, C. Ten, and K. P. Schneider, "Inference of tampered smart meters with validations from feeder-level power injections," in *2019 IEEE Innovative Smart Grid Technologies - Asia (ISGT Asia)*, pp. 2783–2788, 2019.

[77] T. Chen, B. Zhang, H. Pourbabak, A. Kavousi-Fard, and W. Su, "Optimal routing and charging of an electric vehicle fleet for high-efficiency dynamic transit systems," *IEEE Trans on Smart Grid*, vol. 9, no. 4, pp. 3563–3572, 2016.

[78] T. Chen and W. Su, "Indirect customer-to-customer energy trading with reinforcement learning," *IEEE Trans on Smart Grid*, vol. 10, no. 4, pp. 4338–4348, 2018.

[79] Y. Tang, T. Liu, G. Liu, J. Li, R. Dai, and C. Yuan, "Enhancement of power equipment management using knowledge graph," in *IEEE Innovative Smart Grid Technologies - Asia (ISGT Asia)*, pp. 905–910, May 2019.

[80] W. Yuan, J. Wang, F. Qiu, C. Chen, C. Kang, and B. Zeng, "Robust optimization-based resilient distribution network planning against natural disasters," *IEEE Trans on Smart Grid*, vol. 7, no. 6, pp. 2817–2826, 2016.

[81] D. N. Trakas and N. D. Hatziargyriou, "Optimal distribution system operation for enhancing resilience against wildfires," *IEEE Trans on Power Systems*, vol. 33, no. 2, pp. 2260–2271, 2018.

[82] Z. Liang and Y. Guo, "Smart charging and parking of plug-in hybrid electric vehicles in microgrids considering renewable energy sources," in *48th Annual Frontiers of Power Conference*, pp. 1–6, IEEE, 2015.

[83] T. Chen, H. Pourbabak, Z. Liang, W. Su, and P. Yu, "Participation of electric vehicle parking lots into retail electricity market with evoucher mechanism," in *IEEE Conference on Transportation Electrification Asia-Pacific (ITEC Asia-Pacific)*, pp. 1–5, IEEE, 2017.

[84] T. Chen, H. Pourbabak, Z. Liang, and W. Su, "An integrated evoucher mechanism for flexible loads in real-time retail electricity market," *IEEE Access*, vol. 5, pp. 2101–2110, 2017.

[85] Z. Liang and Y. Guo, "Robust optimization based bidding strategy for virtual power plants in electricity markets," in *Power and Energy Society General Meeting (PESGM), 2016*, pp. 1–5, IEEE, 2016.

[86] H. Pourbabak, S. Xu, T. Chen, Z. Liang, and W. Su, "Distributed control algorithm for optimal power allocation of ev parking lots," in *Power and Energy Society General Meeting*, pp. 1–5, IEEE, 2017.

[87] W. Su and M.-Y. Chow, "Performance evaluation of an eda-based large-scale plug-in hybrid electric vehicle charging algorithm," *IEEE Trans on Smart Grid*, no. 99, pp. 1–1, 2011.

[88] W. Su and J. Wang, "Energy management systems in microgrid operations," *The Electricity Journal*, vol. 25, no. 8, pp. 45–60, 2012.

[89] Y. Tang, S. Zhao, C. Ten, K. Zhang, and T. Logenthiran, "Establishment of enhanced load modeling by correlating with occupancy information," *IEEE Trans on Smart Grid*, vol. 11, no. 2, pp. 1702–1713, 2020.

[90] Z. Liang, T. Chen, H. Pourbabak, and W. Su, "Robust distributed energy resources management for microgrids in a retail electricity market," in *Power Symposium (NAPS), 2017 North American*, pp. 1–6, IEEE, 2017.

[91] A. Ajao, J. Luo, Z. Liang, Q. H. Alsafasfeh, and W. Su, "Intelligent home energy management system for distributed renewable generators, dispatchable residential loads and distributed energy storage devices," in *Renewable Energy Congress (IREC), 2017 8th International*, pp. 1–6, IEEE, 2017.

[92] W. Su, "The role of customers in the us electricity market: Past, present and future," *The Electricity Journal*, vol. 27, no. 7, pp. 112–125, 2014.

[93] Z. Liang, D. Bian, D. Su, R. Diao, D. Shi, Z. Wang, and W. Su, "Adaptive robust energy management strategy for campus-based commercial buildings considering comprehensive comfort levels," in *2019 IEEE Power & Energy Society General Meeting (PESGM)*, pp. 1–5, IEEE, 2019.

[94] A. Kavousi-Fard, T. Niknam, and M. Fotuhi-Firuzabad, "A novel stochastic framework based on cloud theory and theta-modified bat algorithm to solve the distribution feeder reconfiguration," *IEEE Trans on Smart Grid*, vol. 7, no. 2, pp. 740–750, 2016.

[95] Y. Tang, *Anomaly Inference Based on Heterogeneous Data Sources in an Electrical Distribution System*. PhD thesis, Michigan Tech University, Houghton, November 2018.

[96] Z. Liang, A. Kavousifard, and W. Su, "Resilient restoration for distribution system operators when facing extreme events," in *2018 North American Power Symposium (NAPS)*, pp. 1–6, IEEE, 2018.